

Meet-in-the-Middle Preimage Attacks on Sponge-based Hashing

Abstract. The Meet-in-the-Middle (MitM) attack has been widely applied to preimage attacks on Merkle-Damgård (MD) hashing. In this paper, we introduce a generic framework of the MitM attack on sponge-based hashing. We find certain bit conditions can significantly reduce the diffusion of the unknown bits and lead to longer MitM characteristics. To find good or optimal configurations of MitM attacks, e.g., the bit conditions, the neutral sets, and the matching points, we introduce the bit-level MILP-based automatic tools on **Keccak**, **Ascon** and **Xoodyak**. To reduce the scale of bit-level models and make them solvable in reasonable time, a series of properties of the targeted hashing are considered in the modelling, such as the linear structure and CP-kernel for **Keccak**, the Boolean expression of Sbox for **Ascon**. Finally, we give an improved 4-round preimage attack on **Keccak-512/SHA3**, and break a nearly 10 years' cryptanalysis record. We also give the first preimage attacks on 3-/4-round **Ascon-XOF** and 3-round **Xoodyak-XOF**.

Keywords: MitM · Automatic Tool · Keccak/SHA3 · Ascon · Xoodyak

1 Introduction

The Meet-in-the-Middle (MitM) attack proposed by Diffie and Hellman in 1977 [21] is a generic technique for cryptanalysis of symmetric-key primitives. The essence of the MitM attack is actually an efficient way to exhaustively search a space for the right candidate based on the birthday attack, i.e., dividing the whole space into two independent subsets (also known as neutral sets) and then finding matches from the two subsets. Suppose $E_K(\cdot)$ to be a block cipher whose size is n -bit such that $C = E_K(P) = F_{K_2}(F_{K_1}(P))$, where $K = K_1 \| K_2$ has n bits, and K_1 and K_2 are independent key materials of $n/2$ bits. For a given plaintext-ciphertext pair (P, C) , a naive exhaust search attack needs a time complexity 2^n to find the key. However, the birthday-paradox based MitM attack computes independently $F_{K_1}(P)$ and $F_{K_2}^{-1}(C)$ with independent guesses of K_1 and K_2 , and searches collision between $F_{K_1}(P)$ and $F_{K_2}^{-1}(C)$ to find the K with a time complexity about $2^{n/2}$. In the past decades, the MitM attack has been widely applied to the cryptanalysis on block ciphers [49, 29, 12, 39] and hash functions [57, 2, 33]. In the meantime, various techniques have been introduced to improve the framework of MitM attack, such as internal state guessing [29], splice-and-cut [2], initial structure [57], bicliques [11], 3-subset MitM [12], indirect-partial matching [2, 57], sieve-in-the-middle [14], match-box [31], dissection [23], differential-aided MitM [40, 30], etc. Till now, the MitM attack and its

39 variants have broken MD4 [43,33], MD5 [57], KeeLoq [38], HAVAL [4,58], GOST
 40 [39], GEA-1/2 [7,1], etc.

41 At CRYPTO 2011 and 2016, several ad-hoc automatic tools [13,18] were pro-
 42 posed for MitM attacks. At IWSEC 2018, Sasaki [55] introduced MILP-based
 43 MitM attacks on GIFT block cipher. At EUROCRYPT 2021, Bao et al. [5] intro-
 44 duced the MILP-based automatic search framework for MitM preimage attacks
 45 on AES-like hashing, whose compression function is built from AES-like block
 46 cipher or permutations. At CRYPTO 2021, Dong et al. [27] further extended
 47 Bao et al.’s model into key-recovery and collision attacks. At CRYPTO 2022,
 48 Schrottenloher and Stevens [59] simplified the language of the automatic model
 49 and applied it in both classic and quantum settings. Bao et al. [6] considered the
 50 MitM attack in a view of the superposition states.

51 When applying to hash functions, most of the MitM attacks targeted on
 52 Merkle-Damgård [50,16] domain extender, whose compression function is usu-
 53 ally built from a block cipher and PGV hashing modes [53], such as Davies-Meyer
 54 (DM), Matyas-Meyer-Oseas (MMO) and Miyaguchi-Preneel (MP). The goal of
 55 the MitM attack is to find a sequence of internal states which satisfy a closed
 56 computational path: there is a relation between the value before the first round
 57 and the value after the last round in previous applications of MitM attacks. For
 58 example, when attacking block-cipher based hashing modes (DM, MMO, MP,
 59 etc.), the closed computation path is computed across the first and last rounds
 60 via the feed-forward mechanism of the hashing modes. While when attacking
 61 block ciphers, the closed computation path is linked via an encryption/decryp-
 62 tion oracle. As shown in Figure 1, one starts by separating the path in two
 63 chunks (splice-and-cut): the backward chunk and the forward chunk depending
 64 on different neutral sets. Both chunks form independent computation paths. One
 65 then finds a partial match between them at certain round.

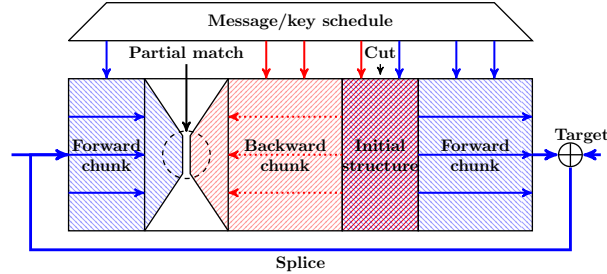


Fig. 1: The closed computation path of the MitM attack

66 When considering the new hashing mode, i.e., sponge-based hashing, there
 67 is no feed-forward mechanism anymore, e.g. Keccak. We have to try novel ways
 68 to build the so-called closed computational path for MitM attack. Most preim-
 69 age attacks on sponge-based hashing focus on the analysis on Keccak/SHA-3
 70 with linearization technique. At ASIACRYPT 2016, Guo et al. [34] introduced
 71 the *linear structure* technique to linearise several rounds of Keccak and derived
 72 upto 4-round preimage attacks. Later, Guo et al.’s attacks were improved by the

73 cross-linear structure [45] at ToSC 2017 and *allocating approach* [44] at EURO-
 74 CRYPT 2019. Further improvements in this line were proposed in [54,36,47,46].
 75 At EUROCRYPT 2021, Dinur [22] gave the preimage attacks on **Keccak** by
 76 solving multivariate equation systems. Additionally, theoretical preimage attacks
 77 marginally better than exhaustive attacks were studied in [8,51].

78 At INDOCRYPT 2011, an MitM attack on 2-round **Keccak** is given by Naya-
 79 Plasencia et al. [52]. However, their MitM attack is different from what we are
 80 considering. In [52], after computing the inverse of one round **Keccak** from the
 81 target, partial internal states are known. Then, Naya-Plasencia et al. divide the
 82 message block into many independent parts and compute forward independently
 83 for each part until the known internal states, and filter the messages. Naya-
 84 Plasencia et al.’s attack is more like a divide-and-conquer and the birthday
 85 attack is not used.

86 **Our Contributions.**

87 We apply the birthday-paradox based MitM attack¹, which has been widely
 88 used to attack Merkle-Damgård [50,16] hashing with PGV modes as well as
 89 block ciphers, to the sponge-based hash functions. Additionally, by applying bit
 90 conditions, the diffusion of the two neutral sets can be controlled and reduced,
 91 and therefore lead to longer MitM characteristics. Finally, we propose a generic
 92 MitM framework with conditions for sponge-based hash functions.

93 To apply our framework to **Keccak**, **Ascon-XOF** and **Xoodyak-XOF**, we have
 94 to search sound configurations for MitM attack, including the choice of the two
 95 neutral sets, the bit conditions, the matching points etc. As **Keccak**, **Ascon** are
 96 bit-level hashing, we introduce the bit-level MILP-based automatic tools to de-
 97 tect those configurations. Different from the previous byte-level MitM MILP
 98 models [5,27,59], the bit-level modelling usually leads to huge scale MILP mod-
 99 els and makes it hard to solve in reasonable time. Therefore, we explore detailed
 100 properties of dedicated ciphers to reduce the models. For **Keccak**, we apply the
 101 linear structures in starting states and CP-kernel properties in matching phase.
 102 For **Ascon**, the Boolean expressions of the Sbox are explored in the starting
 103 states and matching points. In previous modellings [5,27], cells depending on
 104 both two neutral sets are always regarded as useless and unknown in the MitM
 105 attack. The unknown cells can significantly reduce the number of known cells
 106 when propagating (somewhat like polluting), since any known cells will become
 107 unknown by operating with the unknown cells. *Inspired by the indirect-partial*
 108 *matching technique* [2,57], *the cells depending on the additions of the two neu-*
 109 *tral sets are also useful and should not be regarded as unknown in the automatic*
 110 *searching models*. Therefore, we introduce new constraints for those kinds of cells
 111 and reduce the polluting speed of the unknown cells.

112 At last, we derive a better 4-round preimage attack on **Keccak/SHA3-512**
 113 than Morawiecki et al.’s rotational cryptanalysis [51] at FSE 2013, that breaks

¹The Demirci-Selçuk MitM attacks [17,28,19,20,10] are not considered in this paper, which is a quite different technique.

their nearly 10 years' record. While previous preimage attack on **Keccak-512** with linear structure techniques [34] (including improvements with various techniques [47,35,54]) only reaches 3 rounds. For **Ascon-XOF**, the first 3-round and 4-round preimage attacks are given. For **Xoodyak-XOF**, the first 3-round preimage attack is given. A summary of the related results are given in Table 1.

Table 1: A Summary of the Attacks. Lin. Stru.: Linear Structure. MitM: MitM Attack. Diff.: Differential. †: this attack ignores the padding bits.

Target	Attacks	Methods	Rounds	Time	Memory	Ref.
Keccak-512	Preimage	Lin.Stru.	2	2^{384}	-	[34]
		Lin.Stru.	2	2^{321}	-	[54]
		Lin.Stru.	2	2^{270}	-	[47]
		Lin.Stru.	2	2^{252}	-	[35]
		Lin.Stru.	3	2^{482}	-	[34]
		Lin.Stru.	3	2^{475}	-	[54]
		Lin.Stru.	3	2^{452}	-	[47]
		Lin.Stru.	3	2^{426}	-	[35]
		Rotational	4	2^{506}	-	[51]
		MitM	4	$2^{504.58}$	2^{108}	Sect. 4
Xoodyak-XOF	Preimage	Neural	1	-	-	[48]
		MitM	3	$2^{125.06}$	2^{97}	Sect. 5
	Preimage	MitM	3	$2^{120.58}$	2^{39}	Sect. E
		MitM	4	$2^{126.4}$	2^{45}	Sect. 6.2
Ascon-XOF	Preimage	Algebraic†	6	$2^{127.3}$	-	[26]
	Collision	Diff.	2	2^{103}	-	[32]
		Diff.	3	Practical	-	[24]

Comparison to Schrottenloher and Stevens's MitM attack. At CRYPTO 2022, Schrottenloher and Stevens [59] introduced preimage attacks on **SPHINCS++-Haraka** [3], which is sponge-based hashing with permutation **Haraka** [42]. Their MitM attack computes from the two ends, i.e., the known inner part and the target, to the middle matching part. Combining with the guess-and-determine technique, they derived a 3.5-round (out of 5 rounds) quantum preimage attack on **SPHINCS++-Haraka**. As stated in [59, Section 3.1], their frameworks do not lead to interesting results on **Ascon** [26]. The reason may be that for **Keccak** or **Ascon** the inverse of one round is not as easy as **Haraka**. Our framework mainly uses the forward computation, and leads to novel results on both **Keccak** and **Ascon**.

2 Preliminaries

In the section, we give some brief descriptions of the Meet-in-the-Middle attack, the sponge-based hash function, the **Keccak-f** permutation, **Ascon-Hash** and **Ascon-XOF**, **Xoodyak** and **Xoodoo** permutation.

2.1 The Meet-in-the-Middle Attack

Since the pioneering works on preimage attacks on Merkle–Damgård hashing, e.g. MD4, MD5, and HAVAL [43,57,2,33], techniques such as *splice-and-cut* [2], *initial structure* [57] and *indirect-partial matching* have been invented to significantly improve the MitM approach. As shown in Figure 1, in the MitM attack, the compression function is divided at certain intermediate rounds (initial structure) into two chunks. One chunk is computed forward (named as forward chunk), and the other is computed backward (named as backward chunk). One of them is computed across the first and last rounds via the feed-forward mechanism of the hashing mode, and they end at a common intermediate round (partial matching point) and form a closed computation path of the MitM attack. In each of the chunks, the computation involves at least one distinct message word (or a few bits of it), such that they can be computed over all possible values of the involved message word(s) independently from the message word(s) involved in the other chunk (the distinct words are called neutral words). In the initial structure, the two chunks overlapped and the neutral words for both chunks appear simultaneously, but still, the computations of the two chunks on the neutral words are independent. The highlevel framework is in Figure 1, which can be divided into three configurations:

1. The chunk separation – the positions of initial structure and matching points.
2. The neutral sets – the selection on the two neutral sets (denoted as \blacksquare or \blacksquare sets), which determines the degree of freedom (DoF) for each chunk.
3. The matching – the deterministic relation used for matching, which determines the filtering ability (degree of matching, DoM).

After setting up the configurations, the basic attack procedure goes as follows.

1. Choose constants for the initial structure.
2. For all 2^{d_1} values of \blacksquare neutral set, compute backward from the initial structure to the matching points to generate a table L_1 , whose indices are the values for matching, and the elements are the values of \blacksquare neutral set.
3. Similarly, build L_2 for 2^{d_2} values of \blacksquare neutral set with forward computation.
4. Check whether there is an m -bit match on indices between L_1 and L_2 .
5. For the pairs surviving the partial match, check for a full-state match. Steps 1-5 will be repeated until we find a full match.

The attack complexity. Denote the size of the target by h , and the number of bits for the match by m . An MitM episode is performed with time $2^{\max(d_1, d_2)} + 2^{d_1+d_2-m}$ and the total time complexity of the attack is:

$$2^{h-(d_1+d_2)} \cdot (2^{\max(d_1, d_2)} + 2^{d_1+d_2-m}) \simeq 2^{h-\min(d_1, d_2, m)}. \quad (1)$$

To illustrate how the MitM attack works, we detail the 7-round attack on AES-hashing of Sasaki [56] in Supplementary Material A as an example.

2.2 The Sponge-based Hash Function

The sponge construction [9] shown in Figure 2 takes a variable-length message as input and produces a digest of any desired length. The b -bit internal state is composed of an outer part of r bits and an inner part of c bits, where r is the rate and c is the capacity. To evaluate the sponge function, one proceeds in three phases with an inner permutation f :

1. **Initialization:** Initialize the b -bit state with the given value (all 0's for Keccak) before proceeding the message blocks.
2. **Absorbing:** The message is padded and split into blocks of r bits. Absorb each r -bit block M_i by XORing into the internal state.
3. **Squeezing:** Produce the digest.

We named the hash functions with sponge construction as the sponge-based hash functions, e.g. Keccak [9], Ascon [26], Xoodyak [15], to name a few.

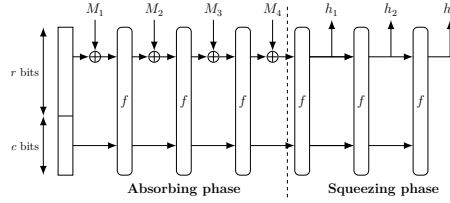


Fig. 2: The sponge construction

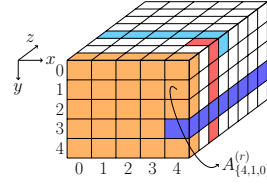


Fig. 3: The Keccak state

2.3 The Keccak- f Permutations

The Keccak hash function family [9] specifies 7 Keccak permutations, denoted Keccak- $f[b]$, where $b \in \{25, 50, 100, 200, 400, 800, 1600\}$ is the width of the permutation. In this paper, we focus on Keccak- $f[1600]$, where the state A is arranged as 5×5 64-bit lanes as depicted in Figure 3. Let $A_{\{x,y,z\}}^{(r)}$ denote the bit located at the x -th column, y -th row and z -th lane in the round r ($r \geq 0$), where $0 \leq x \leq 4$, $0 \leq y \leq 4$, $0 \leq z \leq 63$. For Keccak in the rest of this paper, all the coordinates are considered modulo 5 for x and y and modulo 64 for z . The function Keccak- $f[1600]$ consists of 24 rounds which consists of five operations $\iota \circ \chi \circ \pi \circ \rho \circ \theta$. Denote the internal states of round r as

$$A^{(r)} \xrightarrow{\theta} \theta^{(r)} \xrightarrow{\rho} \rho^{(r)} \xrightarrow{\pi} \pi^{(r)} \xrightarrow{\chi} \chi^{(r)} \xrightarrow{\iota} A^{(r+1)}.$$

Operations in each round are:

$$\begin{aligned}
\theta: \quad \theta_{\{x,y,z\}}^{(r)} &= A_{\{x,y,z\}}^{(r)} \oplus \sum_{y'=0}^4 (A_{\{x-1,y',z\}}^{(r)} \oplus A_{\{x+1,y',z-1\}}^{(r)}), \\
\rho: \quad \rho_{\{x,y,z\}}^{(r)} &= \theta_{\{x,y,z-\gamma[x,y]\}}^{(r)}, \\
\pi: \quad \pi_{\{y,2x+3y,z\}}^{(r)} &= \rho_{\{x,y,z\}}^{(r)}, \\
\chi: \quad \chi_{\{x,y,z\}}^{(r)} &= \pi_{\{x,y,z\}}^{(r)} \oplus (\pi_{\{x+1,y,z\}}^{(r)} \oplus 1) \cdot \pi_{\{x+2,y,z\}}^{(r)}, \\
\iota: \quad A^{(r+1)} &= \chi^{(r)} \oplus RC_r,
\end{aligned} \tag{2}$$

where $\gamma[x, y]$'s are constants given in Table 4 of Supplementary Material B, RC_r is round-dependent constant.

The Keccak and SHA3 Hash Function. The Keccak hash function follows the sponge construction. For $\text{Keccak}[r, c, d]$, the capacity is c , the bitrate is r and the diversifier is d . NIST standardized four SHA3- l versions ($l \in 224, 256, 384, 512$), where $c = 2l$ and $r = 1600 - 2l$. The only difference of Keccak and SHA3 is the padding rule. The padding rule for Keccak is padding the message with '10*1', which is a single bit 1 followed by the minimum number of 0 bits followed by a single bit 1, to make the whole length to a multiple of $(1600 - 2l)$. For SHA3, the message is padded with '0110*1'. However, the padding rule does not affect the final time complexity of our attack.

2.4 Ascon-Hash and Ascon-XOF

The Ascon family [26] includes the hash functions Ascon-Hash and Ascon-Hasha as well as the extendable output functions Ascon-XOF and Ascon-XOFa with sponge-based modes of operations.

Ascon Permutation. The inner permutation applies 12 round functions to a 320-bit state. The state A is split into five 64-bit words, and denote $A_{\{x,y\}}^{(r)}$ to be the x -th (column) bit of the y -th (row) 64-bit word, where $0 \leq y \leq 4$, $0 \leq x \leq 63$. The round function consists of three operations p_C , p_S and p_L . Denote the internal states of round r as $A^{(r)} \xrightarrow{p_S \circ p_C} S^{(r)} \xrightarrow{p_L} A^{(r+1)}$.

- **Addition of Constants p_C :** $A_{\{*,2\}}^{(r)} = A_{\{*,2\}}^{(r)} \oplus RC_r$.
- **Substitution Layer p_S :** For each x , this step updates the columns $A_{\{x,*\}}^{(r)}$ using the 5-bit Sbox. Assume the S-box maps $(a_0, a_1, a_2, a_3, a_4) \in \mathbb{F}_2^5$ to $(b_0, b_1, b_2, b_3, b_4) \in \mathbb{F}_2^5$, where a_0 is the most significant bit. The algebraic normal form (ANF) of the Sbox is as follows:

$$\begin{aligned} b_0 &= a_4a_1 + a_3 + a_2a_1 + a_2 + a_1a_0 + a_1 + a_0, \\ b_1 &= a_4 + a_3a_2 + a_3a_1 + a_3 + a_2a_1 + a_2 + a_1 + a_0, \\ b_2 &= a_4a_3 + a_4 + a_2 + a_1 + 1, \\ b_3 &= a_4a_0 + a_4 + a_3a_0 + a_3 + a_2 + a_1 + a_0, \\ b_4 &= a_4a_1 + a_4 + a_3 + a_1a_0 + a_1. \end{aligned} \tag{3}$$

- **Linear Diffusion Layer p_L :**

$$\begin{aligned} A_{\{*,0\}}^{(r+1)} &\leftarrow S_{\{*,0\}}^{(r)} \oplus (S_{\{*,0\}}^{(r)} \ggg 19) \oplus (S_{\{*,0\}}^{(r)} \ggg 28), \\ A_{\{*,1\}}^{(r+1)} &\leftarrow S_{\{*,1\}}^{(r)} \oplus (S_{\{*,1\}}^{(r)} \ggg 61) \oplus (S_{\{*,1\}}^{(r)} \ggg 39), \\ A_{\{*,2\}}^{(r+1)} &\leftarrow S_{\{*,2\}}^{(r)} \oplus (S_{\{*,2\}}^{(r)} \ggg 1) \oplus (S_{\{*,2\}}^{(r)} \ggg 6), \\ A_{\{*,3\}}^{(r+1)} &\leftarrow S_{\{*,3\}}^{(r)} \oplus (S_{\{*,3\}}^{(r)} \ggg 10) \oplus (S_{\{*,3\}}^{(r)} \ggg 17), \\ A_{\{*,4\}}^{(r+1)} &\leftarrow S_{\{*,4\}}^{(r)} \oplus (S_{\{*,4\}}^{(r)} \ggg 7) \oplus (S_{\{*,4\}}^{(r)} \ggg 41). \end{aligned}$$

221 **Ascon-Hash and Ascon-XOF.** The state A is composed of the outer part with 64
 222 bits $A_{\{*,0\}}$ and the inner part 256 bits $A_{\{*,i\}}$ ($i = 1, 2, 3, 4$). For **Ascon-Hash**, the
 223 output size is 256 bits, and the security claim is 2^{128} . For **Ascon-XOF**, the output
 224 can have arbitrary length and the security claim against preimage attack is
 225 $\min(2^{128}, 2^l)$, where l is the output length. In this paper, we target on **Ascon-XOF**
 226 with a 128-bit hash value and a 128-bit security claim against preimage attack.

227 2.5 Xoodoo and Xoodoo Permutation

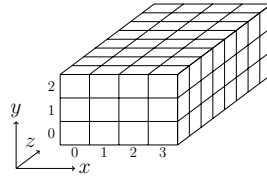


Fig. 4: Toy version of the Xoodoo state. The order in y is opposite to Keccak

228 Internally, **Xoodyak** makes use of the **Xoodoo** permutation [15], whose state
 229 (shown in Figure 4) bit denoted by $A_{\{x,y,z\}}^{(r)}$ is located at the x -th column, y -th
 230 row and z -th lane in the round r , where $0 \leq x \leq 3$, $0 \leq y \leq 2$, $0 \leq z \leq 31$. For
 231 **Xoodoo**, all the coordinates are considered modulo 4 for x , modulo 3 for y and
 232 modulo 32 for z . The permutation consists of the iteration of a round function
 233 $R = \rho_{\text{east}} \circ \chi \circ \iota \circ \rho_{\text{west}} \circ \theta$. The number of rounds is a parameter, which is 12 in
 234 **Xoodyak**. Denote the internal states of the round r as

$$\begin{aligned}
 & A^{(r)} \xrightarrow{\theta} \theta^{(r)} \xrightarrow{\rho_{\text{west}}} \rho^{(r)} \xrightarrow{\iota} \iota^{(r)} \xrightarrow{\chi} \chi^{(r)} \xrightarrow{\rho_{\text{east}}} A^{(r+1)}. \\
 & \theta : \theta_{\{x,y,z\}}^{(r)} = A_{\{x,y,z\}}^{(r)} \oplus \sum_{y'=0}^2 (A_{\{x-1,y',z-5\}}^{(r)} \oplus A_{\{x-1,y',z-14\}}^{(r)}), \\
 & \rho_{\text{west}} : \rho_{\{x,0,z\}}^{(r)} = \theta_{\{x,0,z\}}^{(r)}, \rho_{\{x,1,z\}}^{(r)} = \theta_{\{x-1,1,z\}}^{(r)}, \rho_{\{x,2,z\}}^{(r)} = \theta_{\{x,2,z-11\}}^{(r)}, \\
 & \iota : \iota_{\{0,0,z\}}^{(r)} = \rho_{\{0,0,z\}}^{(r)} \oplus RC_r, \text{ where } RC_r \text{ is round-dependent constant,} \\
 & \chi : \chi_{\{x,y,z\}}^{(r)} = \iota_{\{x,y,z\}}^{(r)} \oplus (\iota_{\{x,y+1,z\}}^{(r)} \oplus 1) \cdot \iota_{\{x,y+2,z\}}^{(r)}, \\
 & \rho_{\text{east}} : A_{\{x,0,z\}}^{(r+1)} = \chi_{\{x,0,z\}}^{(r)}, A_{\{x,1,z\}}^{(r+1)} = \chi_{\{x,1,z-1\}}^{(r)}, A_{\{x,2,z\}}^{(r+1)} = \chi_{\{x-2,2,z-8\}}^{(r)}.
 \end{aligned} \tag{4}$$

236 **Xoodyak** can serve as a XOF, i.e. **Xoodyak-XOF**, which offers arbitrary output
 237 length l . The preimage resistance is $\min(2^{128}, 2^l)$. We target on **Xoodyak-XOF**
 238 with output of 128-bit hash value and 128-bit absorbed message block.

239 3 Meet-in-the-Middle Attack on Sponge-based Hashing

240 The essence of the Meet-in-the-Middle attack is actually an efficient way to
 241 exhaustively search a space for the right one based on the birthday attack. Taken
 242 the MitM attack on DM construction (Figure 5(a)) as an example, suppose

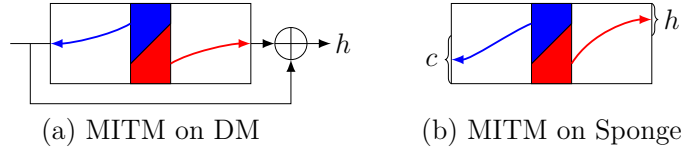


Fig. 5: Differences in MitM attack on PGV and sponge hash functions

the size of the internal state is n , the size of the output is h ($n \geq h$). In the perspective of exhaust search attack, one chooses a random internal state to verify if it leads to the given h -bit target. After searching a space of 2^h internal states, one will find the preimage. In the MitM attacks, as shown in Figure 5(a), the attacker starts from the internal state in the middle, which is divided into two independent forward and backward chunks (marked in red and blue, respectively). One computes the two chunks independently until the matching point to filter the wrong internal states. The details are given in Section 2.1.

When considering the sponge-based hashing, if we start from some similar internal states in the middle (as shown in Figure 5(b)) to search preimage with the given target, the internal state has to satisfy not only the target in forward computation, but also the c -bit inner part in backward computation. In other words, we have to search a space with $2^{(h+c)}$ internal states to meet the target and the inner part. Taking the complexity of exhaustive search (i.e., 2^h) into consideration, it may be not a good idea to search a $(h+c)$ -bit space even with MitM. For sponge-based hashing, we do not follow the conventional start-from-the-middle way to drive the MitM attack. We try to search a more compact space to find the preimage. In fact, we choose to search the r -bit outer part. With the known c -bit inner part, a search of h -bit subspace of the outer part (if $r > h$) with MitM method is enough to find the preimage. The highlevel framework of the MitM approach is shown in Figure 6 and highlighted in the green box. Since we start from the outer part and try to satisfy the h -bit target, only forward computations are involved. Like the MitM attack in Section 2.1, we need to specify the configurations: the two neutral sets of the outer part, the two independent forward computation chunks, the matching points. We may partially solve the inverse of the permutation from the h -bit target to get some internal bits. Thereafter, by forward computing the two independent chunks until those internal bits, the deterministic relations on the two neutral sets were established, which act as the matching point.

3.1 The Conditions in the MitM Attack

The key point of the MitM is to extend the number of rounds of the independent computation path for blue or red neutral words. For Keccak, we have $\chi : b_i = a_i \oplus (a_{i+1} \oplus 1) \cdot a_{i+2}$. Supposing a_{i+1} is blue neutral word and a_i is red neutral word, then b_i depends on both blue and red neutral words if $a_{i+2} = 1$, otherwise b_i only depends on the red neutral words a_i . That is what we called “conditions”.

Setting conditions to control the characteristic can trace back to Wang et al.'s collision attacks with message modification techniques [60,61]. Then, conditions are applied to enhance the probability of the differentials, i.e., the conditional differential cryptanalysis [41]. Later, conditions are used to reduce the diffusion of the cube variables in dynamic cube attack [25] and conditional cube attacks [37]. In MitM attack, the conditions were used to build MitM attacks [57,2] on MD/SHA hashing with ARX structure. For modular addition $X + Y = Z$ ($X, Y, Z \in \mathbb{F}_2^{32}$), particularly the computation of i -th and $(i+1)$ -th bits, assume that the carry from $(i-1)$ -th bit to i -th bit is 0. Then, the $(i+1)$ -th bit of Z is computed as $Z_{\{i+1\}} = X_{\{i+1\}} \oplus Y_{\{i+1\}} \oplus X_{\{i\}} \cdot Y_{\{i\}}$. When $X_{\{i+1\}}$ is blue neutral word and $Y_{\{i\}}$ is red neutral word, the idea of making $X_{\{i\}} = 0$ as a condition so that $Z_{\{i+1\}}$ is only affected by blue neutral word.

In this paper, we try to apply conditions to reduce the diffusion of the red/blue neutral words, and expect to find longer MitM characteristics. In our MitM attack on sponge-based hashing, the conditions usually depend on bits from both inner part (capacity) and outer part (rate). In order to modify certain conditions, we have to modify bits from the inner part. Therefore, as shown in Figure 6, we place the MitM attack in the processing of the last message block and modify the conditions determined by inner part by randomly changing the first several message blocks (e.g. M_1 in Figure 6). Suppose there are μ conditions only determined by the inner part², the probability to find one right M_1 satisfying all the conditions is about $2^{-\mu}$.

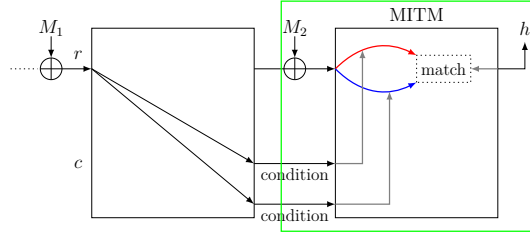


Fig. 6: Framework of the MitM attack on sponge-based hashing

Once we find one right M_1 , we assign arbitrary values to all bits except those neutral bits for M_2 . Then, an MitM episode is performed:

1. Suppose the two neutral sets of the outer part are of 2^{d_1} and 2^{d_2} values, respectively, which are marked by the ■ and ■ color. For each of 2^{d_1} values, compute forward to the matching points.
2. For each of 2^{d_2} values, compute forward to the matching points.
3. Compute backward with the known h -bit target to the matching points to derive an m -bit matching.
4. Filter states.

²Note that, if the conditions are determined by both outer part and inner part, then for given inner part, it is possible to change the message block (i.e., M_2 in Figure 6) to modify the conditions.

The complexity of the MitM episode is $2^{\max(d_1, d_2)} + 2^{d_1+d_2-m}$, which actually checks $2^{d_1+d_2} M_2$. In order to find a preimage of h , we have to repeat the episode for $2^{h-(d_1+d_2)}$ times. After the conditions in inner part are satisfied, suppose there are 2^η non-neutral bits in M_2 that provide 2^η MitM episodes. If $\eta + d_1 + d_2 < h$, we have to find $2^{h-(\eta+d_1+d_2)} M_1$, which all satisfy the conditions in the inner part of the last permutation. The total time complexity is

$$2^{h-(\eta+d_1+d_2)} \cdot 2^\mu + 2^{h-(d_1+d_2)} \cdot (2^{\max(d_1, d_2)} + 2^{d_1+d_2-m}). \quad (5)$$

4 MitM Preimage Attack on Keccak

This section first gives some techniques and properties in previous preimage attacks on Keccak. Then we propose our MILP model for the MitM attack on Keccak. As an application, we mount a 4-round preimage attack on Keccak-512.

4.1 Preliminaries on Keccak

Most previous preimage attacks on Keccak/SHA3 are with the linearization technique. The *linear structure technique allows to linearize the underlying permutation of Keccak for several rounds*. In our attack, we also apply the *linear structure* technique proposed by Guo et al. [34] to linearize one round of Keccak, in order to speed up the search.

Linear Structure. We give an example to explain the *linear structure* technique. As shown in Fig. 7, the variables $v_{0,z}$ and $v_{1,z}$ ($0 \leq z \leq 63$) are allocated as $A_{\{0,0,z\}}^{(0)} = v_{0,z}$, $A_{\{0,1,z\}}^{(0)} = v_{0,z} \oplus c_{0,z}$, $A_{\{2,0,z\}}^{(0)} = v_{1,z}$, $A_{\{2,1,z\}}^{(0)} = v_{1,z} \oplus c_{1,z}$, where $c_{0,z}$ and $c_{1,z}$ ($0 \leq z \leq 63$) are constants. After the θ operation, the variables will not diffuse. After the π operation, any two variables are not adjacent in a row, and all outputs of $A^{(1)}$ are linear. To further reduce the diffusion of the variables in χ operation, one can add restricted constraints to the value of constant bits. For example, for the row $\pi_{\{*,0,z\}}$, setting two bit conditions $\pi_{\{1,0,z\}}^{(0)} = 0$ and $\pi_{\{4,0,z\}}^{(0)} = 1$, the other bits except $A_{\{0,0,z\}}^{(1)}$ in $A_{\{*,0,z\}}^{(1)}$ will be constants. Those conditions can be satisfied by modifying the message block and inner part.

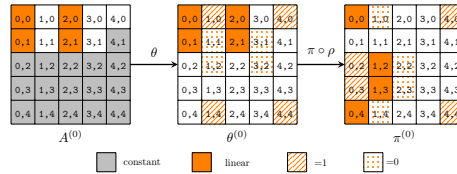


Fig. 7: The linear structure of 1-round Keccak-512

335 **Properties of the Sbox χ .** Guo et al. proposed several properties of the Sbox
 336 χ , which help to mount preimage attacks on Keccak [34]. Those properties can be
 337 also applied in our MitM attack, so we give a brief introduction in the following.
 338 Assume $\chi : \mathbb{F}_2^5 \rightarrow \mathbb{F}_2^5$ maps $(a_0, a_1, a_2, a_3, a_4)$ to $(b_0, b_1, b_2, b_3, b_4)$ as

$$b_i = a_i \oplus (a_{i+1} \oplus 1) \cdot a_{i+2}, \quad (6)$$

339 where all indices are modulo 5. The inverse operation χ^{-1} is

$$a_i = b_i \oplus (b_{i+1} \oplus 1) \cdot (b_{i+2} \oplus (b_{i+3} \oplus 1) \cdot b_{i+4}). \quad (7)$$

340 *Property 1.* [34] When there are three known consecutive output bits, two linear
 341 equations of the input bits can be constructed. E.g., assuming that (b_0, b_1, b_2)
 342 are known, two linear equations on (a_0, a_1, a_2, a_3) are constructed as

$$b_0 = a_0 \oplus (b_1 \oplus 1) \cdot a_2, \quad b_1 = a_1 \oplus (b_2 \oplus 1) \cdot a_3. \quad (8)$$

343 4.2 MILP Model of the MitM Preimage Attack on Keccak

344 In previous MILP models [5,27] of the MitM attack, each bit can take one of
 345 the four colors (■, ■, ■, and □). Generally, the □ bits depending on both ■
 346 and ■, are unknown and useless in the MitM attack. In our model, bits whose
 347 Boolean expression depending on the addition of ■ and ■ (not multiplied) can
 348 also be used in our MitM attack, which is known as the *indirect-partial matching*
 349 *technique* [57,2] and ignored by previous automatic models [5,27]. Therefore, we
 350 introduce another color, i.e., ■. In our MILP models, there are five colors (■, ■,
 351 ■, ■, and □). We first introduce a new efficient encoding scheme of those colors.
 352 Applying the *linear structure* technique, we can skip the first round and construct
 353 the model from the second round. Then we model the attribute propagation of
 354 the five colors over the five operations in each round of Keccak. We also model
 355 the matching phase with the CP-kernel for Keccak. With all above works, we
 356 build an automatic MILP model for the MitM preimage attack on Keccak.

357 **Encoding Scheme.** Since there are 5 colors to encode in the MILP model,
 358 the previous 2-bit encoding method [5,27] is not suitable and we introduce a
 359 new 3-bit encoding scheme, i.e., each bit is represented by three 0-1 variables
 360 $(\omega_0, \omega_1, \omega_2)$:

- 361 – Gray ■: $(1, 1, 1)$, global constant bits,
- 362 – Red ■: $(0, 1, 1)$, bits determined by ■ bits and ■ bits of starting state,
- 363 – Blue ■: $(1, 1, 0)$, bits determined by ■ bits and ■ bits of starting state,
- 364 – Green ■: $(0, 1, 0)$, bits determined by ■ bits, ■ bits and ■ bits, but the
 365 expression does not contain the product of ■ and ■ bits,
- 366 – White □: $(0, 0, 0)$, bits dependent on the product of ■ and ■ bits.

367 We set ω_1 to 0 for □ and to 1 for any other color (■, ■, ■, ■). So □ bit can be
 368 quickly detected by the value of ω_1 . Then we set ω_0 to 1 for (■, ■) and to 0 for
 369 other color (■, ■, ■, □). Similarly for ω_2 .

Modelling the Starting State with the Linear Structure Technique.

In the starting state, each of the 1600 bits takes one color of \blacksquare , $\color{red}\blacksquare$ and $\color{blue}\blacksquare$. We allocate variables $\alpha_{\{x,y,z\}}$ and $\beta_{\{x,y,z\}}$ for the bit with index $\{x,y,z\}$, where $\alpha_{\{x,y,z\}} = 1$ if and only if the bit is $\color{blue}\blacksquare$ and $\beta_{\{x,y,z\}} = 1$ if and only if the bit is $\color{red}\blacksquare$. Therefore, we can compute the initial DoF by $\lambda_{\mathcal{B}} = \sum \alpha_{\{x,y,z\}}$, $\lambda_{\mathcal{R}} = \sum \beta_{\{x,y,z\}}$. For Keccak, we apply the 1-round restricted linear structure as the example given in Section 4.1. Denote the starting state after XORing message block by $A^{(0)}$. The bits in $A_{\{0,0,z\}}^{(0)}$, $A_{\{0,1,z\}}^{(0)}$, $A_{\{2,0,z\}}^{(0)}$ and $A_{\{2,1,z\}}^{(0)}$ can be colored as $\color{blue}\blacksquare$ or $\color{red}\blacksquare$. And the remaining bits of $A^{(0)}$ need to be \blacksquare . In order to control the diffusion of θ operation, $A_{\{0,0,z\}}^{(0)}$ and $A_{\{0,1,z\}}^{(0)}$ should be the same color and the $A_{\{0,0,z\}}^{(0)} \oplus A_{\{0,1,z\}}^{(0)}$ should be constant, which consumes one degree of freedom. Similarly for $A_{\{2,0,z\}}^{(0)}$ and $A_{\{2,1,z\}}^{(0)}$. Thereafter, the coloring pattern keeps the same over the first θ operation. Then with the conditions set in $\pi^{(0)}$ as introduced in Section 4.1, we can omit the first χ operation and construct the model from $A^{(1)}$ only considering the linear operation $\pi \circ \rho$ from $A^{(0)}$.

Modelling the Attribute Propagation. The round function of Keccak consists of five operations θ , ρ , π , χ and ι . The linear operations ρ and π only change the position of each bit of the state. The operation ι can be ignored because it will not change the coloring pattern.

Modelling the θ operation. At first, we give the rule of XOR with an arbitrary number of inputs under the new coloring scheme. We name the rule of by XOR-RULE, which involves five rules:

1. XOR-RULE-1: If the inputs have (0,0,0) \square bit, the output is \square .
2. XOR-RULE-2: If the inputs are all (1,1,1) \blacksquare bits, the output is \blacksquare .
3. XOR-RULE-3: If the inputs have (1,1,0) $\color{blue}\blacksquare$ (≥ 1) and \blacksquare (≥ 0) bits, the output will be $\color{blue}\blacksquare$ without consuming DoF, or \blacksquare by consuming one DoF of $\color{blue}\blacksquare$.
4. XOR-RULE-4: If the inputs have (0,1,1) $\color{red}\blacksquare$ (≥ 1) and \blacksquare (≥ 0) bits, the output will be $\color{red}\blacksquare$ without consuming DoF, or \blacksquare by consuming one DoF of $\color{red}\blacksquare$.
5. XOR-RULE-5: If the inputs have (0,1,0) $\color{green}\blacksquare$ bits, or have at least two kinds of $\color{blue}\blacksquare$, $\color{red}\blacksquare$ and $\color{green}\blacksquare$ bits:
 - (a) the output can be $\color{green}\blacksquare$ without consuming DoF.
 - (b) the output can be $\color{blue}\blacksquare$ (or $\color{red}\blacksquare$) by consuming one DoF of $\color{red}\blacksquare$ (or $\color{blue}\blacksquare$).
 - (c) the output can be \blacksquare by consuming one DoF of $\color{red}\blacksquare$ and one DoF of $\color{blue}\blacksquare$.

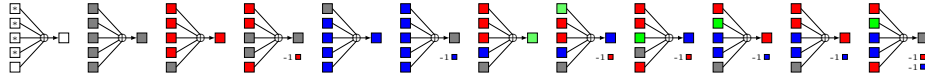


Fig. 8: 5-XOR-RULE (“*” represents the bit can be any color)

We give some valid coloring patterns of 5 inputs of XOR, which are named by 5-XOR-RULE, as shown in Figure 8. Similar to previous MitM attacks [5], we can

use some new variables to identify which rule is applied in different cases. We define three 0-1 variables ν_i ($i \in \{0, 1, 2\}$), where $\nu_0 = 1$ if and only if all the ω_0 's of the 5 input bits are 1, similar to the cases $i = 1, 2$. The above five rules can be represented by (ν_0, ν_1, ν_2) :

1. $(\nu_0, \nu_1, \nu_2) = (*, 0, *)$, XOR-RULE-1 is applied.
2. $(\nu_0, \nu_1, \nu_2) = (1, 1, 1)$, XOR-RULE-2 is applied.
3. $(\nu_0, \nu_1, \nu_2) = (1, 1, 0)$, XOR-RULE-3 is applied.
4. $(\nu_0, \nu_1, \nu_2) = (0, 1, 1)$, XOR-RULE-4 is applied.
5. $(\nu_0, \nu_1, \nu_2) = (0, 1, 0)$, XOR-RULE-5 is applied.

Taking $(\nu_0, \nu_1, \nu_2) = (1, 1, 0)$ as an example. $\nu_1 = 1$ means that all the ω_1 's of the input bits are 1 and there is no \square bit. $\nu_0 = 1$ means that there only may have the \blacksquare or \blacksquare . $\nu_2 = 1$ means that there must have \blacksquare or \blacksquare or \square . Based on the above analysis, we can deduce that when $(\nu_0, \nu_1, \nu_2) = (1, 1, 0)$, there only have \blacksquare and \blacksquare and the number of \blacksquare is greater than or equal to one, where XOR-RULE-3 is applied. Denote the output bit as $(\omega_0^O, \omega_1^O, \omega_2^O)$ and the consumed DoF of \blacksquare bits and \blacksquare bits are $(\delta_{\mathcal{R}}, \delta_{\mathcal{B}})$, we can derive

$$\begin{cases} \omega_0^O - \nu_0 \geq 0, & -\omega_0^O + \nu_1 \geq 0, \\ \omega_1^O - \nu_1 = 0, \\ \omega_2^O - \nu_2 \geq 0, & -\omega_2^O + \nu_1 \geq 0, \end{cases} \quad \begin{cases} \delta_{\mathcal{R}} - \omega_0^O + \nu_0 = 0, \\ \delta_{\mathcal{B}} - \omega_2^O + \nu_2 = 0. \end{cases} \quad (9)$$

In the θ operation, the expression of the output bit is XORing 11 input bits. If we directly compute the XORing value of the 11 input bits, we may double counting the consumption of DoF. For example, given (x, z) , we compute $\theta_{\{x,0,z\}}^{(r)}$ and $\theta_{\{x,1,z\}}^{(r)}$ by $\theta_{\{x,y,z\}}^{(r)} = A_{\{x,y,z\}}^{(r)} \oplus \sum_{y'=0}^4 (A_{\{x-1,y',z\}}^{(r)} \oplus A_{\{x+1,y',z-1\}}^{(r)})$. If bits in the common formula $\sum_{y'=0}^4 (A_{\{x-1,y',z\}}^{(r)} \oplus A_{\{x+1,y',z-1\}}^{(r)})$ are only determined by \blacksquare bits, and $A_{\{x,0,z\}}^{(r)}$, $A_{\{x,1,z\}}^{(r)}$ are \blacksquare bits, we can let the summation bit of $\sum_{y'=0}^4 (A_{\{x-1,y',z\}}^{(r)} \oplus A_{\{x+1,y',z-1\}}^{(r)})$ be \blacksquare by consuming only one DoF of \blacksquare . Thereafter, the two output bits $\theta_{\{x,0,z\}}^{(r)}$, $\theta_{\{x,1,z\}}^{(r)}$ will be \blacksquare . However, if we directly set the two output bits $\theta_{\{x,0,z\}}^{(r)}$, $\theta_{\{x,1,z\}}^{(r)}$ to be \blacksquare by the XOR-RULE individually, we have to consume 2 DoF of \blacksquare . To solve this problem, we depose the θ operation to three steps in our model, as described in the following expressions:

$$\begin{aligned} C_{\{x,z\}}^{(r)} &= A_{\{x,0,z\}}^{(r)} \oplus A_{\{x,1,z\}}^{(r)} \oplus A_{\{x,2,z\}}^{(r)} \oplus A_{\{x,3,z\}}^{(r)} \oplus A_{\{x,4,z\}}^{(r)}, \\ D_{\{x,z\}}^{(r)} &= C_{\{x-1,z\}}^{(r)} \oplus C_{\{x+1,z-1\}}^{(r)}, \\ \theta_{\{x,y,z\}}^{(r)} &= A_{\{x,y,z\}}^{(r)} \oplus D_{\{x,z\}}^{(r)}. \end{aligned}$$

At first, we compute the coloring pattern of $C_{\{x,z\}}^{(r)}$. Then, we compute the coloring pattern of $D_{\{x,z\}}^{(r)}$ and compute $\theta_{\{x,y,z\}}^{(r)}$ at last.

423 *Modelling the χ operation.* For the χ operation in the round 0, we add conditions
 424 to control the diffusion of the ■ or ■ and the first χ is omitted. For the χ operation
 425 from round 1, we build the **SBOX-RULE**. The χ operation maps $(a_0, a_1, a_2, a_3, a_4)$
 426 to $(b_0, b_1, b_2, b_3, b_4)$. According to Equ. (6), $b_i = a_i \oplus (a_{i+1} \oplus 1) \cdot a_{i+2}$. Hence, for
 427 each output bit b_i , we determine its color by (a_i, a_{i+1}, a_{i+2}) :

- 428 1. If there are □ bits in (a_i, a_{i+1}, a_{i+2}) , the output is □.
- 429 2. If there are all ■ bits, the output is ■.
- 430 3. If there are only ■ (≥ 1) and ■ (≥ 0) bits, the output will be ■.
- 431 4. If there are only ■ (≥ 1) and ■ (≥ 0) bits, the output will be ■.
- 432 5. If there are ■, or more than two kinds of ■, ■ and ■ bits in (a_i, a_{i+1}, a_{i+2}) :
 433 (a) if a_{i+1} and a_{i+2} are all ■ (or ■), the output is ■.
 434 (b) if a_{i+1} or a_{i+2} is ■, the output is ■.
 435 (c) if a_{i+1} and a_{i+2} are of arbitrarily two kinds of ■, ■, ■, the output is □.

436 The rules **SBOX-RULE** restrict the coloring pattern of $(a_i, a_{i+1}, a_{i+2}, b_i)$ to the
 437 subset of \mathbb{F}_2^{12} , which is described by the linear inequalities by using the convex
 hull computation. Some valid coloring patterns are shown in Figure 9.

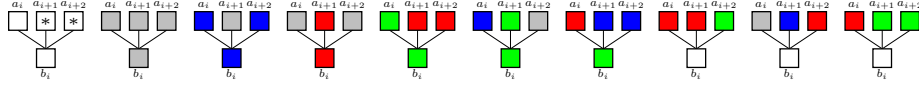


Fig. 9: **SBOX-RULE** for Keccak (“*” represents the bit can be any color)

439 **Modelling Matching Phase.** Suppose the first 512 bits of $A^{(r+1)}$ are the hash
 440 value. In order to attack more rounds, we try to compute certain bits or relations
 441 in $A^{(r)}$ by the hash value in $A^{(r+1)}$, to act as the matching points.

442 *Leaked linear relations of $A^{(r)}$.* From the 512-bit hash, we know $A_{\{*,0,*\}}^{(r+1)}$ and
 443 the first 3 lanes of $A_{\{*,1,*\}}^{(r+1)}$. From $A_{\{*,0,*\}}^{(r+1)}$, we deduce $\pi_{\{*,0,*\}}^{(r)}$ from Equ. (7).
 444 Applying the inverse of the operations ρ and π to $\pi_{\{*,0,*\}}^{(r)}$, we can deduce

$$\theta_{\{x,x,z\}}^{(r)} = \pi_{\{x,0,z+\gamma[x,x]\}}^{(r)}, \forall 0 \leq x \leq 4, 0 \leq z \leq 63. \quad (10)$$

In addition, according to Equ. (8), two linear equations can be deduced from
 the first three bits of each row of $A_{\{*,1,*\}}^{(r+1)}$, which are given as

$$\begin{aligned} A_{\{0,1,z\}}^{(r+1)} &= \pi_{\{0,1,z\}}^{(r)} \oplus (A_{\{1,1,z\}}^{(r+1)} \oplus 1) \cdot \pi_{\{2,1,z\}}^{(r)}, \\ A_{\{1,1,z\}}^{(r+1)} &= \pi_{\{1,1,z\}}^{(r)} \oplus (A_{\{2,1,z\}}^{(r+1)} \oplus 1) \cdot \pi_{\{3,1,z\}}^{(r)}. \end{aligned}$$

445 Then applying the inverse of ρ and π , the linear equations are transformed to

$$\begin{aligned} A_{\{0,1,z\}}^{(r+1)} &= \theta_{\{3,0,z-\gamma[3,0]\}}^{(r)} \oplus (A_{\{1,1,z\}}^{(r+1)} \oplus 1) \cdot \theta_{\{0,2,z-\gamma[0,2]\}}^{(r)}, \\ A_{\{1,1,z\}}^{(r+1)} &= \theta_{\{4,1,z-\gamma[4,1]\}}^{(r)} \oplus (A_{\{2,1,z\}}^{(r+1)} \oplus 1) \cdot \theta_{\{1,3,z-\gamma[1,3]\}}^{(r)}. \end{aligned} \quad (11)$$

446 With the known value $\theta_{\{x,x,z\}}^{(r)}$ ($0 \leq x \leq 4, 0 \leq z \leq 63$) by (10), we add the same
 447 known values (underlined) to both sides of (11), which are

$$\begin{aligned}
 & A_{\{0,1,z\}}^{(r+1)} \oplus \theta_{\{3,3,z-\gamma[3,0]\}}^{(r)} \oplus (A_{\{1,1,z\}}^{(r+1)} \oplus 1) \cdot \theta_{\{0,0,z-\gamma[0,2]\}}^{(r)} \\
 &= \theta_{\{3,0,z-\gamma[3,0]\}}^{(r)} \oplus \theta_{\{3,3,z-\gamma[3,0]\}}^{(r)} \oplus (A_{\{1,1,z\}}^{(r+1)} \oplus 1) \cdot (\theta_{\{0,2,z-\gamma[0,2]\}}^{(r)} \oplus \theta_{\{0,0,z-\gamma[0,2]\}}^{(r)}) \\
 & A_{\{1,1,z\}}^{(r+1)} \oplus \theta_{\{4,4,z-\gamma[4,1]\}}^{(r)} \oplus (A_{\{2,1,z\}}^{(r+1)} \oplus 1) \cdot \theta_{\{1,1,z-\gamma[1,3]\}}^{(r)} \\
 &= \theta_{\{4,1,z-\gamma[4,1]\}}^{(r)} \oplus \theta_{\{4,4,z-\gamma[4,1]\}}^{(r)} \oplus (A_{\{2,1,z\}}^{(r+1)} \oplus 1) \cdot (\theta_{\{1,3,z-\gamma[1,3]\}}^{(r)} \oplus \theta_{\{1,1,z-\gamma[1,3]\}}^{(r)}).
 \end{aligned} \tag{12}$$

448 According to the CP-kernel property [9] of operation θ , we deduce

$$\begin{aligned}
 & \theta_{\{3,0,z-\gamma[3,0]\}}^{(r)} \oplus \theta_{\{3,3,z-\gamma[3,0]\}}^{(r)} = A_{\{3,0,z-\gamma[3,0]\}}^{(r)} \oplus A_{\{3,3,z-\gamma[3,0]\}}^{(r)}, \\
 & \theta_{\{0,2,z-\gamma[0,2]\}}^{(r)} \oplus \theta_{\{0,0,z-\gamma[0,2]\}}^{(r)} = A_{\{0,2,z-\gamma[0,2]\}}^{(r)} \oplus A_{\{0,0,z-\gamma[0,2]\}}^{(r)}, \\
 & \theta_{\{4,1,z-\gamma[4,1]\}}^{(r)} \oplus \theta_{\{4,4,z-\gamma[4,1]\}}^{(r)} = A_{\{4,1,z-\gamma[4,1]\}}^{(r)} \oplus A_{\{4,4,z-\gamma[4,1]\}}^{(r)}, \\
 & \theta_{\{1,3,z-\gamma[1,3]\}}^{(r)} \oplus \theta_{\{1,1,z-\gamma[1,3]\}}^{(r)} = A_{\{1,3,z-\gamma[1,3]\}}^{(r)} \oplus A_{\{1,1,z-\gamma[1,3]\}}^{(r)}.
 \end{aligned} \tag{13}$$

449 Combining (12) and (13), there are linear relations on bits in $A^{(r)}$ with the
 450 known hash value of $A^{(r+1)}$, which will be used in our matching points:

$$\begin{aligned}
 & A_{\{3,0,z-\gamma[3,0]\}}^{(r)} \oplus A_{\{3,3,z-\gamma[3,0]\}}^{(r)} \oplus (A_{\{1,1,z\}}^{(r+1)} \oplus 1) \cdot (A_{\{0,2,z-\gamma[0,2]\}}^{(r)} \oplus A_{\{0,0,z-\gamma[0,2]\}}^{(r)}) \\
 &= A_{\{0,1,z\}}^{(r+1)} \oplus \theta_{\{3,3,z-\gamma[3,0]\}}^{(r)} \oplus (A_{\{1,1,z\}}^{(r+1)} \oplus 1) \cdot \theta_{\{0,0,z-\gamma[0,2]\}}^{(r)},
 \end{aligned} \tag{14}$$

$$\begin{aligned}
 & A_{\{4,1,z-\gamma[4,1]\}}^{(r)} \oplus A_{\{4,4,z-\gamma[4,1]\}}^{(r)} \oplus (A_{\{2,1,z\}}^{(r+1)} \oplus 1) \cdot (A_{\{1,3,z-\gamma[1,3]\}}^{(r)} \oplus A_{\{1,1,z-\gamma[1,3]\}}^{(r)}) \\
 &= A_{\{1,1,z\}}^{(r+1)} \oplus \theta_{\{4,4,z-\gamma[4,1]\}}^{(r)} \oplus (A_{\{2,1,z\}}^{(r+1)} \oplus 1) \cdot \theta_{\{1,1,z-\gamma[1,3]\}}^{(r)}.
 \end{aligned} \tag{15}$$

451 **Observation 1 (Conditions in Matching Points of Keccak)** In (14), if four
 452 bits ($A_{\{3,0,z-\gamma[3,0]\}}^{(r)}, A_{\{3,3,z-\gamma[3,0]\}}^{(r)}, A_{\{0,2,z-\gamma[0,2]\}}^{(r)}, A_{\{0,0,z-\gamma[0,2]\}}^{(r)}$) in $A^{(r)}$ satisfy
 453 the following two conditions, there is a 1-bit filter:

- 454 (1) There has no \square in ($A_{\{3,0,z-\gamma[3,0]\}}^{(r)}, A_{\{3,3,z-\gamma[3,0]\}}^{(r)}, A_{\{0,2,z-\gamma[0,2]\}}^{(r)}, A_{\{0,0,z-\gamma[0,2]\}}^{(r)}$).
 455 (2) ($A_{\{3,0,z-\gamma[3,0]\}}^{(r)}, A_{\{3,3,z-\gamma[3,0]\}}^{(r)}$) is of ($\blacksquare, \blacksquare$), ($\blacksquare, \blacksquare$), ($\blacksquare, \blacksquare$), ($\blacksquare, \blacksquare$), or ($\blacksquare, \blacksquare$), or
 456 opposite order.

457 We introduce a binary variable $\delta_{\mathcal{M}}$ to represent whether there is a filtering.
 458 Similarly to the XOR-RULE, we add three 0-1 variables ν_i ($i \in \{0, 1, 2\}$), where
 459 $\nu_i = 1$ ($i = 0, 2$) if and only if all ω_i 's of ($A_{\{3,0,z-\gamma[3,0]\}}^{(r)}, A_{\{3,3,z-\gamma[3,0]\}}^{(r)}$) are 1,
 460 and $\nu_1 = 1$ if and only if all ω_1 's of ($A_{\{3,0,z-\gamma[3,0]\}}^{(r)}, A_{\{3,3,z-\gamma[3,0]\}}^{(r)}, A_{\{0,2,z-\gamma[0,2]\}}^{(r)}$,
 461 $A_{\{0,0,z-\gamma[0,2]\}}^{(r)}$) are 1. We can derive

$$\begin{cases} \nu_1 - \delta_{\mathcal{M}} \geq 0, & -\nu_0 - \delta_{\mathcal{M}} + 1 \geq 0, & -\nu_2 - \delta_{\mathcal{M}} + 1 \geq 0, \\ \nu_0 - \nu_1 + \nu_2 + \delta_{\mathcal{M}} \geq 0. \end{cases}$$

The Objective Function. Let $l_{\mathcal{R}}$, and $l_{\mathcal{B}}$ be the accumulated consumption of DoF of \blacksquare and \blacksquare , i.e., $l_{\mathcal{R}} = \sum \delta_{\mathcal{R}}$ and $l_{\mathcal{B}} = \sum \delta_{\mathcal{B}}$. Therefore, we can get $\text{DoF}_{\mathcal{R}} = \lambda_{\mathcal{R}} - l_{\mathcal{R}}$, $\text{DoF}_{\mathcal{B}} = \lambda_{\mathcal{B}} - l_{\mathcal{B}}$. We also have $\text{DoM} = \sum \delta_{\mathcal{M}}$. According to the time complexity given by Equ. (1), we need to maximize the value of $\min\{\text{DoF}_{\mathcal{R}}, \text{DoF}_{\mathcal{B}}, \text{DoM}\}$ to find the optimal attacks. We introduce an auxiliary variable v_{obj} , impose the following constraints, and maximize v_{obj} ,

$$\{v_{obj} \leq \text{DoF}_{\mathcal{R}}, v_{obj} \leq \text{DoF}_{\mathcal{B}}, v_{obj} \leq \text{DoM}\}. \quad (16)$$

4.3 MitM Preimage Attack on 4-Round Keccak-512

We follow the framework in Figure 6 to perform the attack with two message blocks (M_1, M_2). The MitM attack is placed at the 2nd block. We construct an MILP model for Keccak-512 following Section 4.2. The source code is given in <https://anonymous.4open.science/r/Conditional-MITM-Preimage-Attack>. By solving with our MILP model, we mount a 4-round MitM preimage attack on Keccak-512, shown in Figure 10,16,17,18, which contains 3 additional symbols:

- $\blacksquare, \blacksquare$: there consumes one degree of freedom of \blacksquare to let the bit be \blacksquare or \blacksquare .
- \blacksquare : there consumes one degree of freedom of \blacksquare to let the bit be \blacksquare .
- \blacksquare : \blacksquare bits used for matching.

Conditions in the Linear Structure. State $A^{(0)}$ contains 16 \blacksquare bits and 216 \blacksquare bits. We take the similar strategy with [47] to get 1-round linear structure of Keccak. We introduce 116 binary variables $v = \{v_0, v_1, \dots, v_{115}\}$ and 116 binary variables $c = \{c_0, c_1, \dots, c_{115}\}$. Those variables v_i 's and c_i 's are placed at the $16 + 216 = 232$ \blacksquare and \blacksquare bits in $A^{(0)}$ in Figure 10,16,17,18. For example, we set $A_{\{0,0,0\}}^{(0)} = v_0$ and $A_{\{0,1,0\}}^{(0)} = v_0 \oplus c_0$. When we choose $c \in \mathbb{F}_2^{116}$ to be arbitrary constant, the θ operation will act as identity with regard to the \blacksquare and \blacksquare bits in $A^{(0)}$. To reduce the diffusion of χ in round 0, we need to set some bits conditions in $\pi^{(0)}$ to be constants. According to (6), if a_{i+1} is \blacksquare or \blacksquare , we need to set $a_{i+2} = 0$ and $a_i = 1$. So there are totally $232 \times 2 = 464$ conditions on $\pi^{(0)}$. After the inverse of $\rho \circ \pi$, we determine the positions of bit conditions in $\theta^{(0)}$. Taking the state $\theta_{\{*,*,1\}}^{(0)}$ as an example, there are six bit conditions as

$$\theta_{\{1,0,1\}}^{(0)} = 1, \theta_{\{1,2,1\}}^{(0)} = 0, \theta_{\{1,4,1\}}^{(0)} = 1, \theta_{\{3,1,1\}}^{(0)} = 0, \theta_{\{3,2,1\}}^{(0)} = 0, \theta_{\{4,4,1\}}^{(0)} = 1. \quad (17)$$

Above conditions can be converted to those on $A^{(0)}$. The bits in $A^{(0)}$ can be divided into two parts: the bits determined by the outer part (i.e., they can be modified by directly changing the absorbed M_2), and the bits determined by

inner part. The equations in Equ. (17) can be transformed to

$$\begin{aligned}
& A_{\{1,0,1\}}^{(0)} \oplus c_2 \oplus A_{\{0,2,1\}}^{(0)} \oplus A_{\{0,3,1\}}^{(0)} \oplus A_{\{0,4,1\}}^{(0)} \oplus c_1 \oplus A_{\{2,2,0\}}^{(0)} \oplus A_{\{2,3,0\}}^{(0)} \oplus A_{\{2,4,0\}}^{(0)} = 1, \\
& A_{\{1,2,1\}}^{(0)} \oplus c_2 \oplus A_{\{0,2,1\}}^{(0)} \oplus A_{\{0,3,1\}}^{(0)} \oplus A_{\{0,4,1\}}^{(0)} \oplus c_1 \oplus A_{\{2,2,0\}}^{(0)} \oplus A_{\{2,3,0\}}^{(0)} \oplus A_{\{2,4,0\}}^{(0)} = 0, \\
& A_{\{1,4,1\}}^{(0)} \oplus c_2 \oplus A_{\{0,2,1\}}^{(0)} \oplus A_{\{0,3,1\}}^{(0)} \oplus A_{\{0,4,1\}}^{(0)} \oplus c_1 \oplus A_{\{2,2,0\}}^{(0)} \oplus A_{\{2,3,0\}}^{(0)} \oplus A_{\{2,4,0\}}^{(0)} = 1, \\
& A_{\{3,1,1\}}^{(0)} \oplus c_3 \oplus A_{\{2,2,1\}}^{(0)} \oplus A_{\{2,3,1\}}^{(0)} \oplus A_{\{2,4,1\}}^{(0)} \oplus A_{\{4,0,0\}}^{(0)} \oplus A_{\{4,1,0\}}^{(0)} \oplus A_{\{4,2,0\}}^{(0)} \oplus A_{\{4,3,0\}}^{(0)} \oplus A_{\{4,4,0\}}^{(0)} = 0, \\
& A_{\{3,2,1\}}^{(0)} \oplus c_3 \oplus A_{\{2,2,1\}}^{(0)} \oplus A_{\{2,3,1\}}^{(0)} \oplus A_{\{2,4,1\}}^{(0)} \oplus A_{\{4,0,0\}}^{(0)} \oplus A_{\{4,1,0\}}^{(0)} \oplus A_{\{4,2,0\}}^{(0)} \oplus A_{\{4,3,0\}}^{(0)} \oplus A_{\{4,4,0\}}^{(0)} = 0, \\
& A_{\{4,4,1\}}^{(0)} \oplus A_{\{3,0,1\}}^{(0)} \oplus A_{\{3,1,1\}}^{(0)} \oplus A_{\{3,2,1\}}^{(0)} \oplus A_{\{3,3,1\}}^{(0)} \oplus A_{\{3,4,1\}}^{(0)} \oplus c_0 \oplus A_{\{0,2,0\}}^{(0)} \oplus A_{\{0,3,0\}}^{(0)} \oplus A_{\{0,4,0\}}^{(0)} = 1, \tag{18}
\end{aligned}$$

where $c_0 = A_{\{0,0,0\}}^{(0)} \oplus A_{\{0,1,0\}}^{(0)}$, $c_1 = A_{\{2,0,0\}}^{(0)} \oplus A_{\{2,1,0\}}^{(0)}$, $c_2 = A_{\{0,0,1\}}^{(0)} \oplus A_{\{0,1,1\}}^{(0)}$, $c_3 = A_{\{2,0,1\}}^{(0)} \oplus A_{\{2,1,1\}}^{(0)}$. Given an inner part, the 464 conditions on state $A^{(0)}$ will be a linear system of the $576 - 116 = 460$ variables of M_2 (marked by bold). We compute the rank of the coefficient matrix of the linear system is 232. In other words, through some linear transformations, there are 232 equations out of the total 464 only determined by the bits of inner part. For example, combining the 2nd and 3rd equations in Equ. (18), we can deduce an equation between two inner part bits $A_{\{1,2,1\}}^{(0)} \oplus A_{\{1,4,1\}}^{(0)} = 1$. We have to randomly test $2^{232} M_1$ to compute the inner part satisfying the 232 equations. Then for a right inner part, there are $2^{460-232} = 2^{228}$ solutions of M_2 , which make all the 464 equations hold. For each solution of M_2 , the \blacksquare and $c \in \mathbb{F}_2^{116}$ in the outer part will be fixed. Then with the fixed inner part, we can conduct the MitM episodes to filter states.

Consumed Degrees of Freedom. As shown in Figure 10,16,17,18, after adding 464 conditions and consuming 108 \blacksquare and 8 \blacksquare degrees of freedom in round 0, we can derive the coloring pattern in $A^{(1)}$. The remaining degrees of freedom for \blacksquare and \blacksquare are 108 and 8, respectively. We give two examples to explain the consumption of degrees of freedom in the computation from $A^{(1)}$ to $A^{(3)}$.

1. For $\theta_{\{0,0,12\}}^{(1)}$ marked by \blacksquare in Figure 11 (part of Figure 10), we set an equation of \blacksquare to a constant, which means consuming one DoF of \blacksquare to let $\theta_{\{0,0,12\}}^{(1)}$ be \blacksquare , as listed below:

$$\begin{aligned}
& A_{\{0,0,12\}}^{(1)} \oplus A_{\{4,0,12\}}^{(1)} \oplus A_{\{4,1,12\}}^{(1)} \oplus A_{\{4,2,12\}}^{(1)} \oplus A_{\{4,3,12\}}^{(1)} \oplus A_{\{4,4,12\}}^{(1)} \\
& \oplus A_{\{1,0,11\}}^{(1)} \oplus A_{\{1,1,11\}}^{(1)} \oplus A_{\{1,2,11\}}^{(1)} \oplus A_{\{1,3,11\}}^{(1)} \oplus A_{\{1,4,11\}}^{(1)} = \text{const.}, \tag{19}
\end{aligned}$$

2. For $\theta_{\{1,3,5\}}^{(2)}$ marked by \blacksquare in Figure 12, we set an equation of \blacksquare to a constant, which means consuming one DoF of \blacksquare to let $\theta_{\{1,3,5\}}^{(2)}$ be \blacksquare . Since there have

$$\begin{aligned}
\theta_{\{1,3,5\}}^{(2)} &= A_{\{1,3,5\}}^{(2)} \oplus D_{\{1,5\}}^{(2)} = A_{\{1,3,5\}}^{(2)} \oplus C_{\{0,5\}}^{(2)} \oplus C_{\{2,4\}}^{(2)}, \\
C_{\{0,5\}}^{(2)} &= A_{\{0,0,5\}}^{(2)} \oplus A_{\{0,1,5\}}^{(2)} \oplus A_{\{0,2,5\}}^{(2)} \oplus A_{\{0,3,5\}}^{(2)} \oplus A_{\{0,4,5\}}^{(2)}, \\
C_{\{2,4\}}^{(2)} &= A_{\{2,0,4\}}^{(2)} \oplus A_{\{2,1,4\}}^{(2)} \oplus A_{\{2,2,4\}}^{(2)} \oplus A_{\{2,3,4\}}^{(2)} \oplus A_{\{2,4,4\}}^{(2)}.
\end{aligned}$$

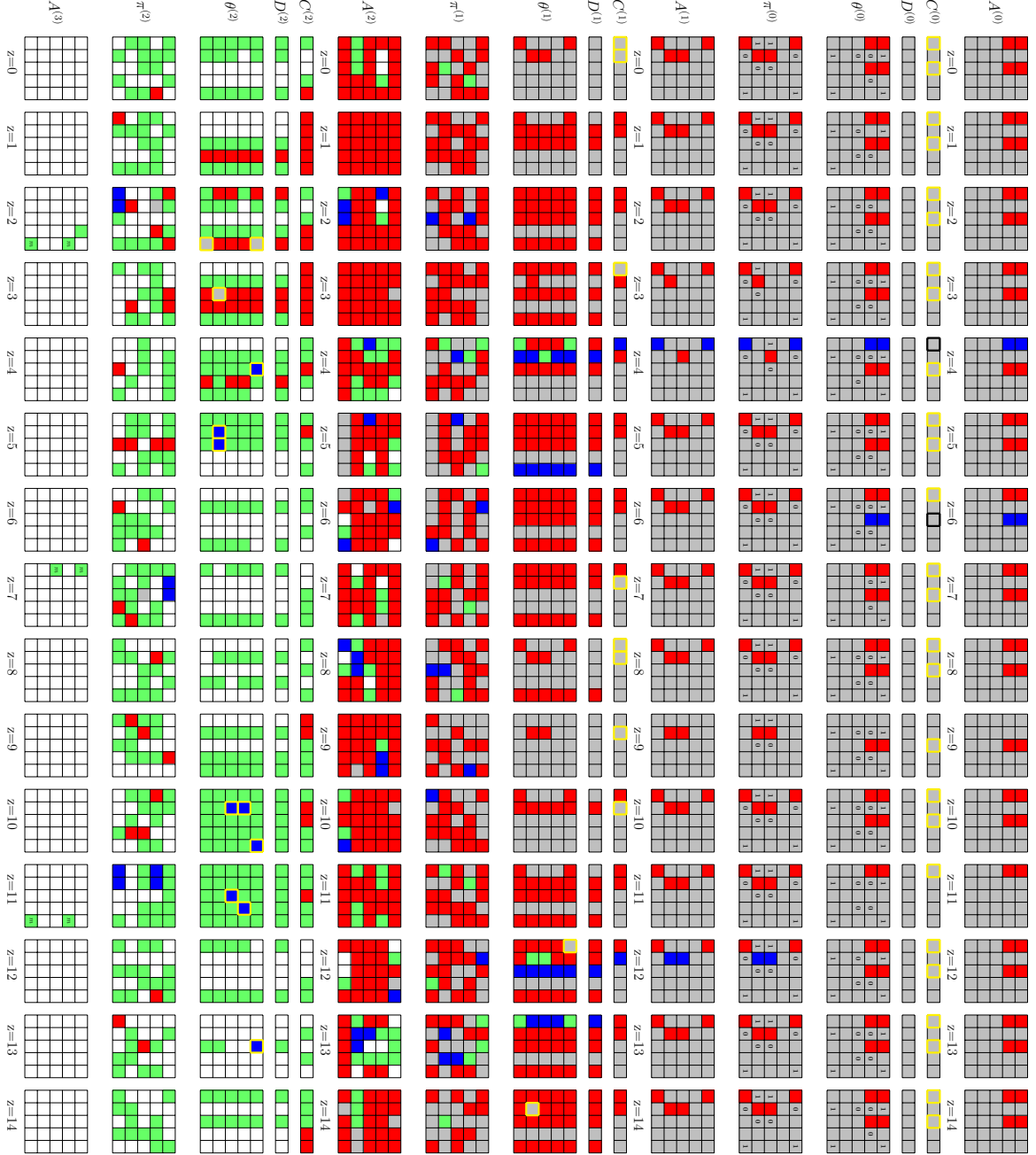


Fig. 10: The MitM preimage attack on 4-round Keccak-512 (part I)

We can set all the \blacksquare involved to be constant:

$$\begin{aligned} & A_{\{1,3,5\}}^{(2)} \oplus A_{\{0,0,5\}}^{(2)} \oplus A_{\{0,1,5\}}^{(2)} \oplus A_{\{0,3,5\}}^{(2)} \oplus A_{\{0,4,5\}}^{(2)} \\ & A_{\{2,0,4\}}^{(2)} \oplus A_{\{2,1,4\}}^{(2)} \oplus A_{\{2,2,4\}}^{(2)} \oplus A_{\{2,3,4\}}^{(2)} \oplus A_{\{2,4,4\}}^{(2)} = \text{const.} \end{aligned} \quad (20)$$

Then, we have $\theta_{\{1,3,5\}}^{(2)} = A_{\{0,2,5\}}^{(2)} \oplus \text{const.}$

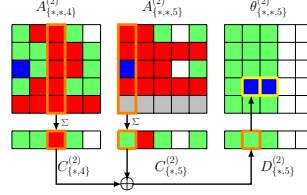
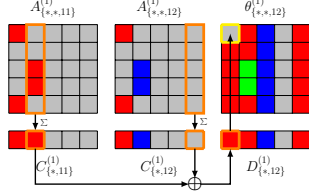


Fig. 11: Example (1) of consumed DoF Fig. 12: Example (2) of consumed DoF

There are totally 100 \blacksquare and \blacksquare in internal states between $A^{(1)}$ and $\theta^{(2)}$, which means that the accumulated consumed degree of freedom of \blacksquare is 100. Denote the 100-bit constants (i.e. constants such as (19) and (20)) as $c_{\mathcal{R}} \in \mathbb{F}_2^{100}$. At last, the numbers of remaining degrees of freedom for \blacksquare and \blacksquare are both 8 bits.

Matching Strategy with Green Bits. According to Obs. 1, we can use $A^{(3)}$ to count the number of matching equations, i.e. $m = 8$. We give an example matching Equ. (21) (marked by \blacksquare in $A^{(3)}$ with $z = 2$ and $z = 41$ in Figure 10) according to Equ. (15), which satisfies the matching conditions of Obs. 1:

$$A_{\{4,1,2\}}^{(3)} \oplus A_{\{4,4,2\}}^{(3)} \oplus (A_{\{2,1,22\}}^{(4)} \oplus 1) \cdot (A_{\{1,3,41\}}^{(3)} \oplus A_{\{1,1,41\}}^{(3)}) \oplus A_{\{1,1,22\}}^{(4)} \oplus \theta_{\{4,4,2\}}^{(3)} \oplus (A_{\{2,1,22\}}^{(4)} \oplus 1) \cdot \theta_{\{1,1,41\}}^{(3)} = 0. \quad (21)$$

With known bits in $A^{(4)}$ and $\theta^{(3)}$, the left part of Equ. (21) can be written as Boolean expression (denoted as $f_{\mathcal{M}}$) on \blacksquare , \blacksquare and \blacksquare bits of the starting state. Therefore, denote $f_{\mathcal{M}} = f_{\mathcal{R}} \oplus f_{\mathcal{B}} \oplus f_{\mathcal{G}}$, where $f_{\mathcal{R}}$ only contains monomials on $\blacksquare/\blacksquare$ bits, $f_{\mathcal{B}}$ contains monomials on $\blacksquare/\blacksquare$ bits, and $f_{\mathcal{G}}$ contains monomials on \blacksquare bits and constants. With the given \blacksquare bits, we can compute the value $f_{\mathcal{R}} \oplus f_{\mathcal{G}} = f'_{\mathcal{M}}$ with forward computing Keccak permutation by setting all the \blacksquare bits as 0. Similarly, we get $f_{\mathcal{B}} \oplus f_{\mathcal{G}} = f''_{\mathcal{M}}$ by setting \blacksquare bits as 0. By setting all \blacksquare and \blacksquare bits as 0, we get $f_{\mathcal{G}} = f'''_{\mathcal{M}}$. Therefore, we compute $f_{\mathcal{R}} = f'_{\mathcal{M}} \oplus f'''_{\mathcal{M}}$ and $f_{\mathcal{B}} = f''_{\mathcal{M}} \oplus f'''_{\mathcal{M}}$. Then, we can derive the matching equation from Equ. (21) as $f_{\mathcal{R}} = f_{\mathcal{B}} \oplus f_{\mathcal{G}}$.

MitM Attack on 4-round Keccak-512. In our attack Algorithm 1 in Figure 10,16,17,18, we first precompute inversely from the target $A^{(4)}$ to $A^{(3)}$, and derive 128 Boolean equations with similar form with Equ. (21). Among them, 8 Boolean equations act as the matching points in the MitM phase, and the other 120 Boolean equations are used to further filter the partial matched states.

Following the framework in Figure 6, we use two message blocks (M_1, M_2) to build the attack as Algorithm 1. In Line 5, once we find solutions of M_2 , we

Algorithm 1: Preimage Attack on 4-round Keccak-512

```

1 Precompute inversely from the target to  $A^{(3)}$ , and derive 128 Boolean
  equations of similar form with Equ. (21)
2 /* Among them, 8 Boolean equations act as the matching points in
   the MitM phase. The other 120 Boolean equations are used to
   further filter the partial matched states. */
3 for  $2^x$  values of  $M_1$  do
4   Compute the inner part of the 2nd block and solve the system of 464
     linear equations
5   if the equations have solutions /* with probability of  $2^{-232}$  */
6     then
7       for each of the  $2^{228}$  solutions of  $M_2$  do
8         /* With  $x = 400$ , there are  $2^{400-232+228} = 2^{396}$  iterations */
9         Compute the  $\blacksquare$  bits in  $A^{(1)}$ 
10        Traversing the  $2^{108}$  values of  $\blacksquare$  in  $A^{(1)}$  while fixing  $\blacksquare$  as 0, compute
          forward to determine 100-bit  $\blacksquare/\blacksquare$  bits (denoted as  $c_{\mathcal{R}} \in \mathbb{F}_2^{100}$ ),
          and the 8-bit matching point, e.g., in (21), i.e., compute eight
           $f'_{\mathcal{M}} = f_{\mathcal{R}} \oplus f_{\mathcal{G}}$ . Build the table  $U$  and store the 108-bit  $\blacksquare$  bits of
           $A^{(1)}$  as well as the 8-bit matching point in  $U[c_{\mathcal{R}}]$ .
11        /* This method to solve the nonlinear constrained neutral
           words is borrowed from Dong et al. [27]. */
12        for  $c_{\mathcal{R}} \in \mathbb{F}_2^{100}$  do
13          Randomly pick a 108-bit  $\blacksquare e \in U[c_{\mathcal{R}}]$ , and set  $\blacksquare$  in  $A^{(1)}$  as 0,
            compute to the matching point to get eight
             $f'''_{\mathcal{M}} = f_{\mathcal{G}} + \text{Const}(e)$ 
14          for  $2^8$  values in  $U[c_{\mathcal{R}}]$  do
15            Restore the values of  $\blacksquare$  of  $A^{(1)}$  and the corresponding
              matching point (i.e., eight  $f_{\mathcal{R}} \oplus f_{\mathcal{G}} = f'_{\mathcal{M}}$ ) in a list  $L_1$ 
              (indexed by matching point)
16          end
17          for  $2^8$  values of  $\blacksquare$  do
18            Set the 108-bit  $\blacksquare$  in  $A^{(1)}$  as  $e$ . Compute to the matching
              point to get eight  $f''_{\mathcal{M}} = f_{\mathcal{B}} + f_{\mathcal{G}} + \text{Const}(e)$ . Together
              with  $f'''_{\mathcal{M}}$ , compute  $f_{\mathcal{B}} = f'_{\mathcal{M}} + f'''_{\mathcal{M}}$  and store  $\blacksquare$  in  $L_2$ 
              indexed by matching point.
19          end
20          for values matched between  $L_1$  and  $L_2$  do
21            Compute  $A^{(3)}$  from the matched  $\blacksquare$  and  $\blacksquare$  bits
22            if  $A^{(3)}$  satisfy the 120 precomputed Boolean
              equations /* Probability of  $2^{-120}$  */
23              then
24                if it leads to the given hash value then
25                  Output the preimage
26                end
27              end
28            end
29          end
30        end
31      end
32 end

```

can perform 2^{100} MitM episodes in Line 14 to 25 for each of the 2^{228} solutions. For each MitM episode, $2^8 \times 2^8$ internal states are exhausted. Suppose there needs 2^x possible values of M_1 . To find a 512-bit target preimage, we need $2^{x-232+228+100+8+8} = 2^{512}$, i.e., $x = 400$. The steps of Algorithm 1 are analyzed below:

- In Line 4, the time complexity is 2^{400} 4-round Keccak and $2^{400} \times 464^3$ bit operations to solve the linear system (the time to solve a system of n linear equations is about $O(n^3)$).
- In Line 9, the time complexity is $2^{400-232+228} \times \frac{1}{4} = 2^{394}$ 4-round Keccak.
- We describe the way to use Equ. (21) as the matching point. In the concrete Keccak attack, we can not set the 108 \blacksquare bits to be 0 when computing $f_B + f_G = f_M''$ and $f_G = f_M'''$. This is because, the actual size of the \blacksquare and \blacksquare neutral sets is both 2^8 , not 2^{108} . The 100 consumed DoF of \blacksquare bits of $A^{(1)}$ are used to make 100 internal bits (denoted as $c_R \in \mathbb{F}_2^{100}$) to be $\blacksquare/\blacksquare$, so that the remaining \blacksquare set of size 2^8 can be computed independent to the \blacksquare set. We detail the method to derive similar matching equation like “ $f_R = f_B \oplus f_G$ ” or “ $f_B = f_R \oplus f_G$ ” for the two 2^8 $\blacksquare/\blacksquare$ sets. With fixed \blacksquare bits in $A^{(1)}$ and $c_R \in \mathbb{F}_2^{100}$, there are 2^8 \blacksquare bits stored in $U[c_R]$, which is derived in Line 10 of Algorithm 1 following Dong et al.’s method [27]. Setting \blacksquare in $A^{(1)}$ as 0, for each element of $U[c_R]$, compute forward the Keccak permutation to the 8 matching bit equations (e.g. Equ. (21)) to get 8 $f_M' = f_R \oplus f_G$ for matching. Randomly pick an element e of $U[c_R]$ and set \blacksquare in $A^{(1)}$ as 0, to compute the 8 matching equations $f_M''' = f_G + \text{Const}(e)$, where $\text{Const}(e)$ is determined by e . That is, for each of the 2^8 \blacksquare , compute $f_M'' = f_B + f_G + \text{Const}(e)$ by setting the 108 \blacksquare $A^{(1)}$ bits as e . Therefore, we get $f_M'' + f_M''' = f_B = f_R \oplus f_G = f_M'$ as filter. To dive into details, we refer the readers to Line 10 to Line 25.
- In Line 10, the time complexity is $2^{396+108} \times \frac{2}{4} = 2^{503}$ 4-round Keccak, since only two rounds from $A^{(1)}$ to $A^{(3)}$ are needed to compute to derive the $\blacksquare/\blacksquare$ bits and the matching points.
- In Line 13, the time complexity is $2^{396+100} \times \frac{2}{4} = 2^{495}$ 4-round Keccak.
- In Line 15, this step is just to retrieve $U[c_R]$ to restore it in L_1 with matching point as index. Suppose one access to the table is equivalent to one Sbox application. The time complexity is $2^{396+100+8} \times \frac{1}{4 \times 320} = 2^{493.36}$ 4-round Keccak, since there are 4×320 Sboxes for 4-round Keccak.
- In Line 18, the time complexity is $2^{396+100+8} \times \frac{2}{4} = 2^{503}$ 4-round Keccak.
- In Line 21, the time is $2^{396+100+8+8-8} \times \frac{2}{4} = 2^{503}$ 4-round Keccak.
- In Line 22, $A^{(3)}$ is checked against the 120 Boolean equations precomputed in Line 1, which acts as a filter of 2^{-120} . After the filter, the time of the final check against the target h is $2^{396+100+8-120} = 2^{384}$ 4-round Keccak.

The total complexity is $2^{400} + 2^{400} \times 464^3 + 2^{394} + 2^{503} + 2^{495} + 2^{493.36} + 2^{503} + 2^{384} \approx 2^{504.58}$ 4-round Keccak. The memory to store U is 2^{108} . We also give an experiment of the MitM episode of 3-round Keccak-512 in the Supplementary Material C.

584 *Remark on padding rule.* The last message block has at least 2-bit padding (i.e.,
 585 ‘11’) for Keccak and 4-bit padding (i.e., ‘0111’) for SHA3. Therefore, we have
 586 $x = 402$ for Keccak-512 and $x = 404$ for SHA3-512. However, it only increases
 587 the negligible part $2^{400} \times 464^3$ in Line 4 to $2^{402} \times 464^3$ for Keccak-512 and
 588 $2^{404} \times 464^3$ for SHA3-512. Therefore the final time complexity is still $2^{504.58}$
 589 4-round Keccak-512 or SHA3-512 considering the padding. The memory is 2^{108}
 590 to store U .

591 5 MitM Preimage Attack on Xoodyak-XOF

592 The Xoodyak is based on Xoodoo permutation, which is inspired by Keccak- f
 593 permutation. The MILP model for Xoodyak is similar with that for Keccak in
 594 Section 4.2. The size of absorbed message block of Xoodyak-XOF is 128 bits. We
 595 target on Xoodyak-XOF with output of 128-bit hash (like the case for Ascon-XOF).
 596 In this section, we list the differences in the MILP model and give an MitM
 597 preimage attack on 3-round Xoodyak-XOF.

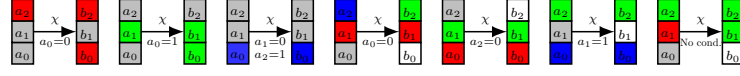
598 5.1 MILP Model of the MitM Preimage Attack on Xoodyak-XOF

599 For Xoodyak, without the help of the *linear structure* technique, the situations of
 600 adding conditions to the state before the Sbox χ are more complex. We give the
 601 details of the condition rules and the matching rule for Xoodyak in the following.

602 **Modelling the χ operation with conditions in Round 0.** The Sbox χ
 603 of Xoodyak is different from that of Keccak at the sizes of inputs and outputs,
 604 which acts on a column $A_{\{x,*,z\}}^{(r)}$. Assume χ operation maps $(a_0, a_1, a_2) \in \mathbb{F}_2^3$ in
 605 to $(b_0, b_1, b_2) \in \mathbb{F}_2^3$ as $b_i = a_i \oplus (a_{i+1} \oplus 1) \cdot a_{i+2}$. In round 0, all the operations
 606 between the starting state $A^{(0)}$ and χ are linear, thus the inputs only have ■, ■,
 607 ■ and ■. We can add conditions on ■ bits to control the diffusion. The different
 608 rules from the SBOX-RULE for Keccak are listed below:

- 609 1. If there are two ■ bits and one ■/■/■ bit in (a_0, a_1, a_2) , we can add one or two
 610 conditions to make one or two outputs to be ■. Without losing generality,
 611 suppose a_i is ■ or ■ or ■ and both a_{i+1} and a_{i+2} are ■ bits:
 - 612 (a) the color of b_i is always same with a_i .
 - 613 (b) $a_{i+2} = 1$, b_{i+1} will be ■; otherwise, the color of b_{i+1} will be same with a_i .
 - 614 (c) $a_{i+1} = 0$, b_{i+2} will be ■; otherwise, the color of b_{i+2} will be same with a_i .
- 615 2. If there is only one ■ bit and the other two are among $(\text{red}, \text{blue})/(\text{red}, \text{green})/(\text{blue}, \text{green})$,
 616 we add conditions to reduce the number of ■ in the output. If a_i is ■:
 - 617 (a) b_i is always be □.
 - 618 (b) $a_i = 0$, the color of b_{i+1} will be same with a_{i+1} and b_{i+2} will be ■.
 - 619 (c) $a_i = 1$, b_{i+1} will be ■ and the color of b_{i+2} will be same with a_{i+2} .
 - 620 (d) without conditions on a_i , both b_{i+1} and b_{i+2} will be ■.

621 The rules can be described by a system of linear inequalities by using the convex
 622 hull computation. Some valid coloring patterns are shown in Figure 13.

Fig. 13: Some valid coloring patterns with conditions for χ

Modelling the Matching Degrees. Suppose the 128 bits in the top plane $A_{\{*,2,*\}}^{(r+1)}$ of $A^{(r+1)}$ is the hash value. We can easily compute the top plane of state $\chi_{\{*,2,*\}}^{(r)}$ from the hash value by the inverse of ρ_{east} . Each bit of $\chi_{\{*,2,*\}}^{(r)}$ is computed by $b_2 = a_2 \oplus (a_0 \oplus 1) \cdot a_1$, where (a_0, a_1, a_2) comes from the input column of each Sbox in $\iota^{(r)}$. Hence, we deduce the deterministic relations of $\iota^{(r)}$ to count the DoMs.

Observation 2 (Conditions in Matching Points of Xoodyak) *If (a_0, a_1, a_2) satisfy the following conditions, we say there is a 1-bit matching:*

1. There is no \blacksquare bit in (a_0, a_1, a_2) .
2. There is no the product of \blacksquare and \blacksquare , concretely, (a_0, a_1) should not be $(\blacksquare, \blacksquare)$ or $(\blacksquare, \blacksquare)$ or $(\blacksquare, \blacksquare)$ or $(\blacksquare, \blacksquare)$, or opposite order.
3. In fact, (a_0, a_1, a_2) should be $(\blacksquare, *, \blacksquare)$ or $(*, \blacksquare, \blacksquare)$ or $(\blacksquare, \blacksquare, \blacksquare)$ or $(\blacksquare, \blacksquare, \blacksquare)$ or $(\blacksquare, \blacksquare, \blacksquare)$ or $(\blacksquare, \blacksquare, \blacksquare)$, where ‘ $*$ ’ is \blacksquare or \blacksquare or \blacksquare or \blacksquare . We exclude several cases such as $(\blacksquare, \blacksquare, \blacksquare)$, since it is a filter if $\blacksquare = 1$, but not for $\blacksquare = 0$.

5.2 MitM Preimage Attack on 3-round Xoodyak-XOF

We also follow the similar framework in Figure 6 and perform the attack with two message blocks (M_1, M_2) , where M_2 has two padding bits ‘10’. The MitM attack is placed in the 2nd block. Solving with our MILP model for Xoodyak, we get a 3-round MitM preimage attack as shown in Figure 23 in Supplementary Material D. Similar to Keccak, we decompose the θ operation into three steps, where $C_{\{x,z\}}^{(r)} = \sum_{y'=0}^2 A_{\{x,y',z\}}^{(r)}$, $D_{\{x,z\}}^{(r)} = C_{\{x-1,z-5\}}^{(r)} \oplus C_{\{x-1,z-14\}}^{(r)}$, and $\theta_{\{x,y,z\}}^{(r)} = A_{\{x,y,z\}}^{(r)} \oplus D_{\{x,z\}}^{(r)}$. The starting state $A^{(0)}$ contains 4 \blacksquare bits and 97 \blacksquare bits. There are totally 53 conditions on \blacksquare bits of $\iota^{(0)}$, which are listed in Table 2. In the computation from $A^{(0)}$ to $\iota^{(2)}$, the accumulated consumed degree of freedom of \blacksquare is 93 and there is no DoF of \blacksquare consumed. Therefore, $\text{DoF}_{\mathcal{B}} = 4$, $\text{DoF}_{\mathcal{R}} = 97 - 93 = 4$. The degree of matching is counted by the deterministic relations of $\iota^{(2)}$ according to Observation 2, we get $\text{DoM} = 4$, where

$$\begin{aligned} \chi_{\{2,2,4\}}^{(2)} &= \ell_{\{2,2,4\}}^{(2)} \oplus (\ell_{\{2,0,4\}}^{(2)} \oplus 1) \cdot \ell_{\{2,1,4\}}^{(2)}, \chi_{\{1,2,10\}}^{(2)} = \ell_{\{1,2,10\}}^{(2)} \oplus (\ell_{\{1,0,10\}}^{(2)} \oplus 1) \cdot \ell_{\{1,1,10\}}^{(2)}, \\ \chi_{\{1,2,19\}}^{(2)} &= \ell_{\{1,2,19\}}^{(2)} \oplus (\ell_{\{1,0,19\}}^{(2)} \oplus 1) \cdot \ell_{\{1,1,19\}}^{(2)}, \chi_{\{2,2,22\}}^{(2)} = \ell_{\{2,2,22\}}^{(2)} \oplus (\ell_{\{2,0,22\}}^{(2)} \oplus 1) \cdot \ell_{\{2,1,22\}}^{(2)}. \end{aligned} \quad (22)$$

In the starting state $A^{(0)}$, there are $128 - 2 - 97 - 4 = 25$ \blacksquare bits which can be modified by changing M_2 . Similar to the conditions of Keccak, the 53 conditions can form a linear system taking these 25 bits of M_2 as variables and the 256 bits inner part as constants. The rank of the coefficient matrix is 13. Therefore,

we have to randomly test $2^{(53-13)} = 2^{40}$ M_1 to satisfy the 40 equations only determined by the inner part. Then for a right inner part, there are $2^{25-13} = 2^{12}$ solutions of M_2 , which make all the 53 equations hold. The attack is similar to the attack on **Keccak**, and we list it in the Algorithm 3 in Supplementary Material **D**. In the MitM episode in Line 10 to 22, a space of 2^{4+4} is searched. In order to search a 128-bit preimage, we have to search a space of $2^{x-40+12+93+8} = 2^{128}$, i.e., $x = 55$. Each step of Algorithm 3 is analyzed below:

- In Line 2, the time complexity is $2^{55} \times 53^3 = 2^{72.2}$ bit operations and 2^{55} 3-round **Xoodyak**.
- In Line 7, the time complexity is $2^{27+97} \times \frac{128+128+4}{128 \times 3} = 2^{123.44}$ 3-round **Xoodyak**. The fraction $\frac{128+128+4}{128 \times 3}$ is because that in the last round only 4 Sboxes with matching points are computed, while there are totally 128×3 Sboxes applications in the 3-round **Xoodyak**.
- In Line 9, the time is $2^{27+93} \times \frac{128+128+4}{128 \times 3} = 2^{119.44}$ 3-round **Xoodyak**.
- In Line 11, the time is $2^{27+93+4} \times \frac{1}{320} = 2^{115.68}$ 3-round **Xoodyak**. This step is just to retrieve the values $U[c_{\mathcal{R}}]$ and restore it in L_1 . Assuming one table access is about one Sbox application, we get the fraction $\frac{1}{320}$.
- In Line 14, the time is $2^{27+93+4} \times \frac{128+128+4}{128 \times 3} = 2^{123.44}$ 3-round **Xoodyak**.
- In Line 17, the time complexity is $2^{27+93+4} \times \frac{2}{3} = 2^{123.42}$ 3-round **Xoodyak**.
- In Line 18, we only compute 5 Sboxes with $\iota^{(2)}$ to gain a filter of 2^{-5} , whose time complexity is $2^{27+93+4} \times \frac{5}{128 \times 3} = 2^{117.74}$ 3-round **Xoodyak**.
- In Line 21, we check the remaining states with the remaining $128-4-5 = 119$ Sboxes, which is $2^{27+93+4-5} \times \frac{119}{384} = 2^{117.31}$ 3-round **Xoodyak**.

The total complexity of the 3-round attack is $2^{72.2} + 2^{55} + 2^{123.44} + 2^{119.44} + 2^{115.68} + 2^{123.44} + 2^{123.42} + 2^{117.74} + 2^{117.31} \approx 2^{125.06}$ 3-round **Xoodyak-XOF**, and the memory to store U is 2^{97} .

$\iota_{\{0,0,3\}}^{(0)} = 0; \iota_{\{0,1,3\}}^{(0)} = 1; \iota_{\{1,0,3\}}^{(0)} = 0; \iota_{\{2,0,3\}}^{(0)} = 0; \iota_{\{3,1,4\}}^{(0)} = 1; \iota_{\{3,2,5\}}^{(0)} = 1;$
$\iota_{\{2,0,6\}}^{(0)} = 0; \iota_{\{2,1,6\}}^{(0)} = 1; \iota_{\{3,0,6\}}^{(0)} = 0; \iota_{\{3,1,6\}}^{(0)} = 1; \iota_{\{2,0,7\}}^{(0)} = 1; \iota_{\{3,1,7\}}^{(0)} = 0; \iota_{\{3,2,7\}}^{(0)} = 1;$
$\iota_{\{2,2,8\}}^{(0)} = 0; \iota_{\{2,0,8\}}^{(0)} = 1; \iota_{\{3,0,10\}}^{(0)} = 0; \iota_{\{3,0,11\}}^{(0)} = 0; \iota_{\{3,1,11\}}^{(0)} = 1; \iota_{\{1,0,12\}}^{(0)} = 0; \iota_{\{1,1,12\}}^{(0)} = 1;$
$\iota_{\{0,0,13\}}^{(0)} = 0; \iota_{\{0,1,13\}}^{(0)} = 1; \iota_{\{3,0,13\}}^{(0)} = 0; \iota_{\{3,1,13\}}^{(0)} = 1; \iota_{\{2,0,14\}}^{(0)} = 0; \iota_{\{2,0,15\}}^{(0)} = 0;$
$\iota_{\{3,0,15\}}^{(0)} = 0; \iota_{\{3,1,15\}}^{(0)} = 1; \iota_{\{0,1,19\}}^{(0)} = 1; \iota_{\{3,0,19\}}^{(0)} = 0; \iota_{\{2,1,20\}}^{(0)} = 0; \iota_{\{3,0,20\}}^{(0)} = 0; \iota_{\{3,1,20\}}^{(0)} = 1;$
$\iota_{\{0,0,21\}}^{(0)} = 1; \iota_{\{2,2,21\}}^{(0)} = 0; \iota_{\{3,1,21\}}^{(0)} = 0; \iota_{\{3,2,21\}}^{(0)} = 1; \iota_{\{2,0,22\}}^{(0)} = 1; \iota_{\{2,2,22\}}^{(0)} = 0; \iota_{\{3,1,22\}}^{(0)} = 0;$
$\iota_{\{1,0,23\}}^{(0)} = 0; \iota_{\{1,1,23\}}^{(0)} = 1; \iota_{\{0,0,28\}}^{(0)} = 0; \iota_{\{3,0,28\}}^{(0)} = 0; \iota_{\{0,0,29\}}^{(0)} = 0; \iota_{\{0,1,29\}}^{(0)} = 1;$
$\iota_{\{3,0,29\}}^{(0)} = 0; \iota_{\{3,1,29\}}^{(0)} = 1; \iota_{\{0,0,30\}}^{(0)} = 0; \iota_{\{2,2,30\}}^{(0)} = 0; \iota_{\{2,0,31\}}^{(0)} = 1; \iota_{\{2,2,31\}}^{(0)} = 0; \iota_{\{3,1,31\}}^{(0)} = 0$

Table 2: Bit Conditions in 3-round Attack on **Xoodyak-XOF**

6 MitM Preimage Attack on **Ascon-XOF**

In this section, we list the details of the MILP model for **Ascon-XOF** different from that for **Keccak**, and give an MitM preimage attack on 4-round **Ascon-XOF**.

6.1 MILP Model of the MitM Preimage Attack on Ascon-XOF

We do not model Ascon with \blacksquare bit, since the Sbox of Ascon is much more complex than Keccak, and the output of the Sbox will be unknown if there is \blacksquare bit in the input in most cases. The \blacksquare bit can hardly improve the modelling of Ascon. The other modellings are similar to Keccak, we only list the differences.

Modelling the Starting State with Conditions. In the starting state $A^{(0)}$, the 64-bit outer part can be \blacksquare or \blacksquare bits, while the last 256-bit inner part is of \blacksquare . As shown in the first two cases in Figure 14, p_S maps $(a_0, a_1, a_2, a_3, a_4)$ to $(b_0, b_1, b_2, b_3, b_4)$, where the a_0 in the outer part could be \blacksquare or \blacksquare and (a_1, a_2, a_3, a_4) in the inner part are always \blacksquare . When a_0 is \blacksquare and others are \blacksquare , all the output bits excluding b_2 should be \blacksquare according to Equ. (3) (case 1 in Figure 14). However, if we add some conditions on (a_1, a_2, a_3, a_4) , for example $a_1 = 1$ and $a_3 + a_4 = 1$, then according to Equ. (3), b_0 and b_3 can also be \blacksquare (case 2 in Figure 14). We add conditions on the bits in the inner part of $A^{(0)}$ to control the diffusion of \blacksquare and \blacksquare over p_S . We name the rule by CondSBOX-RULE:

1. Condition on a_1 : when $a_1 = 1$, b_0 is \blacksquare and the color of b_4 is the same with a_0 ; when $a_1 = 0$, b_4 is \blacksquare and the color of b_0 is the same with a_0 .
2. Condition on $a_3 + a_4$: when $a_3 + a_4 = 1$, b_3 is \blacksquare ; when $a_3 + a_4 = 0$, the color of b_3 is the same with a_0 .

Some valid coloring patterns of CondSBOX-RULE are shown in Figure 14.

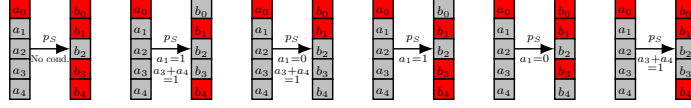


Fig. 14: Some valid red coloring patterns of CondSBOX-RULE (Similar to blue bits)

Modelling the Matching Degree. We target on Ascon-XOF with a 128-bit hash value, which needs two output blocks. Suppose the 64-bit word $A_{\{0,*\}}^{(r+1)}$ of $A^{(r+1)}$ is the first 64-bit hash value of the first output block. We can easily compute the first 64 bits of state $S^{(r)}$ from the hash value by the inverse of p_L . Each of the first 64 bits of $S^{(r)}$ is computed by $b_0 = a_4a_1 + a_3 + a_2a_1 + a_2 + a_1a_0 + a_1 + a_0$ by Equ. (3), where $(a_0, a_1, a_2, a_3, a_4)$ comes from the inputs of each Sbox in $A^{(r)}$. Hence, we deduce the deterministic relations of $A^{(r)}$ to count the degree of freedom of matching.

Observation 3 (Conditions in Matching Points of Ascon) If $(a_0, a_1, a_2, a_3, a_4)$ satisfy the following conditions, we say there is a 1-bit matching:

1. There is no \blacksquare bit in $(a_0, a_1, a_2, a_3, a_4)$.
2. There are \blacksquare and \blacksquare bits in $(a_0, a_1, a_2, a_3, a_4)$.
3. There are no product of \blacksquare and \blacksquare , concretely, (a_1, a_4) should not be $(\blacksquare, \blacksquare)$ or $(\blacksquare, \blacksquare)$, and the same to (a_1, a_2) and (a_0, a_1) .

6.2 MitM Preimage Attack on 4-round Ascon-XOF

Applying the MILP model, we find a 4-round MitM preimage attack as shown in Figure 24 in Supplementary Material E. The starting state $A^{(0)}$ contains 2 ■ bits and 45 ■ bits. There are totally 50 conditions on ■ of $A^{(0)}$, which are listed in Table 3. In the computation from $A^{(0)}$ to $A^{(3)}$, the accumulated consumed degrees of freedom of ■ is 43 and there is no DoF of ■ consumed. Therefore, $\text{DoF}_B = 2$, $\text{DoF}_R = 45 - 43 = 2$. The two matching bit equations ($\text{DoM} = 2$) are derived by $A^{(3)}$ with Observation 3, which are:

$$\begin{cases} A_{\{4,4\}}^{(3)} \cdot A_{\{4,1\}}^{(3)} + A_{\{4,3\}}^{(3)} + A_{\{4,2\}}^{(3)} \cdot A_{\{4,1\}}^{(3)} + A_{\{4,2\}}^{(3)} + A_{\{4,1\}}^{(3)} \cdot A_{\{4,0\}}^{(3)} + A_{\{4,1\}}^{(3)} + A_{\{4,0\}}^{(3)} = S_{\{4,0\}}^{(3)}, \\ A_{\{48,4\}}^{(3)} \cdot A_{\{48,1\}}^{(3)} + A_{\{48,3\}}^{(3)} + A_{\{48,2\}}^{(3)} \cdot A_{\{48,1\}}^{(3)} + A_{\{48,2\}}^{(3)} + A_{\{48,1\}}^{(3)} \cdot A_{\{48,0\}}^{(3)} + A_{\{48,1\}}^{(3)} + A_{\{48,0\}}^{(3)} = S_{\{48,0\}}^{(3)}. \end{cases} \quad (23)$$

$A_{\{1,1\}}^{(0)} = 1; A_{\{3,1\}}^{(0)} = 1; A_{\{4,1\}}^{(0)} = 0; A_{\{5,1\}}^{(0)} = 1; A_{\{6,1\}}^{(0)} = 0; A_{\{8,1\}}^{(0)} = 0; A_{\{9,1\}}^{(0)} = 1;$
$A_{\{12,1\}}^{(0)} = 1, A_{\{12,3\}}^{(0)} + A_{\{12,4\}}^{(0)} = 1; A_{\{15,1\}}^{(0)} = 1; A_{\{18,1\}}^{(0)} = 1, A_{\{18,3\}}^{(0)} + A_{\{18,4\}}^{(0)} = 1;$
$A_{\{19,1\}}^{(0)} = 0; A_{\{22,1\}}^{(0)} = 1, A_{\{22,3\}}^{(0)} + A_{\{22,4\}}^{(0)} = 1; A_{\{23,1\}}^{(0)} = 1; A_{\{26,1\}}^{(0)} = 1;$
$A_{\{28,1\}}^{(0)} = 1, A_{\{28,3\}}^{(0)} + A_{\{28,4\}}^{(0)} = 1; A_{\{29,1\}}^{(0)} = 1; A_{\{30,1\}}^{(0)} = 0, A_{\{30,3\}}^{(0)} + A_{\{30,4\}}^{(0)} = 1;$
$A_{\{31,1\}}^{(0)} = 1; A_{\{32,1\}}^{(0)} = 1; A_{\{33,1\}}^{(0)} = 1; A_{\{35,1\}}^{(0)} = 1, A_{\{35,3\}}^{(0)} + A_{\{35,4\}}^{(0)} = 1; A_{\{38,1\}}^{(0)} = 1;$
$A_{\{39,1\}}^{(0)} = 1, A_{\{39,3\}}^{(0)} + A_{\{39,4\}}^{(0)} = 1; A_{\{40,1\}}^{(0)} = 0, A_{\{40,3\}}^{(0)} + A_{\{40,4\}}^{(0)} = 1; A_{\{41,1\}}^{(0)} = 0;$
$A_{\{44,1\}}^{(0)} = 0; A_{\{45,1\}}^{(0)} = 0; A_{\{47,1\}}^{(0)} = 0, A_{\{47,3\}}^{(0)} + A_{\{47,4\}}^{(0)} = 1; A_{\{48,1\}}^{(0)} = 0;$
$A_{\{50,1\}}^{(0)} = 0, A_{\{50,3\}}^{(0)} + A_{\{50,4\}}^{(0)} = 1; A_{\{51,1\}}^{(0)} = 1; A_{\{53,1\}}^{(0)} = 0;$
$A_{\{54,1\}}^{(0)} = 1, A_{\{54,3\}}^{(0)} + A_{\{54,4\}}^{(0)} = 1; A_{\{59,1\}}^{(0)} = 0, A_{\{59,3\}}^{(0)} + A_{\{59,4\}}^{(0)} = 1;$
$A_{\{60,1\}}^{(0)} = 0, A_{\{60,3\}}^{(0)} + A_{\{60,4\}}^{(0)} = 1; A_{\{61,1\}}^{(0)} = 0, A_{\{61,3\}}^{(0)} + A_{\{61,4\}}^{(0)} = 1$

Table 3: Bit Conditions in 4-round Attack on Ascon-XOF

Following the framework in Figure 6, we choose (M_1, M_2) to make the 50 conditions hold, and perform the MitM attack with the 3rd message block M_3 . The 4-round attack is given in Algorithm 2. In Line 11 to Line 26, a subspace of 2^{2+2} is traversed. In Algorithm 2, to find a 128-bit preimage, we exhaust $2^{x-50+15+43+4} = 2^{128}$, i.e., $x = 116$. The steps of Alg. 2 are analyzed below:

- In Line 3, the time complexity is $2^{116} \times 2 = 2^{117}$ 4-round Ascon.
- In Line 6, there are 15 free bits in M_3 by excluding the 2-bit padding, 45-bit ■ and 2-bit ■ bits.
- In Line 9, the time complexity is $2^{116-50+15} \times \frac{1}{4} = 2^{79}$ 4-round Ascon.
- In Line 10, for each of the 2^{45} ■ bits in $A^{(0)}$, we need compute $45 + 56 + 20 = 121$ out of the total $64 \times 4 = 256$ Sbox applications (4 rounds) to build U . Hence, the time of Line 10 is $2^{116-50+15+45} \times \frac{121}{256} = 2^{124.9}$ 4-round Ascon.
- As U stores red values and matching points, in Line 13, building L_1 is just to retrieve the values in $U[c_R]$. If one table access is about one Sbox application, the time of Line 13 is $2^{116-50+15+43+2} \times \frac{1}{256} = 2^{118}$ 4-round Ascon.
- In Line 16, given ■ bits of $A^{(0)}$, the time to compute the matching points is $2 + 5 + 6 = 13$ Sbox applications. Therefore, the time of Line 16 is $2^{116-50+15+43+2} \times \frac{13}{256} = 2^{121.7}$ 4-round Ascon.

Algorithm 2: Preimage Attack on 4-round Ascon-XOF

```

1  Inversely precompute  $S_{\{*,0\}}^{(3)}$  with the 64-bit hashing value
2  for  $2^x$  values of  $(M_1, M_2)$  do
3      Compute the inner part of the 3rd block
4      if the conditions in Table 3 are satisfied /* probability of  $2^{-50}$  */
5          then
6              for  $2^{64-2-45-2} = 2^{15}$  values of the  $\blacksquare$  bits in  $M_3$ 
7                  /* There are 2-bit padding in  $M_3$  fixed globally */
8                  do
9                      Compute the  $\blacksquare$  bits in  $A^{(0)}$  to  $A^{(1)}$ , except those  $\blacksquare$  bits
10                     Traversing the  $2^{45}$  values for  $\blacksquare$  in  $A^{(0)}$  while fixing  $\blacksquare$  as 0, compute
                        the 43-bit  $\blacksquare/\blacksquare$  bits as  $c_{\mathcal{R}} \in \mathbb{F}_2^{43}$  and store the 45-bit  $\blacksquare$  of  $A^{(0)}$ 
                        and two matching bits (i.e.,  $A_{\{4,1\}}^{(3)} \cdot A_{\{4,0\}}^{(3)} + A_{\{4,1\}}^{(3)} + A_{\{4,0\}}^{(3)} + S_{\{4,0\}}^{(3)}$ ,
                         $A_{\{48,1\}}^{(3)} \cdot A_{\{48,0\}}^{(3)} + A_{\{48,1\}}^{(3)} + A_{\{48,0\}}^{(3)} + S_{\{48,0\}}^{(3)}$ , which are red parts of
                        (23)) in table  $U[c_{\mathcal{R}}]$ .
11                     for  $c_{\mathcal{R}} \in \mathbb{F}_2^{43}$  do
12                         for  $2^2$  values in  $U[c_{\mathcal{R}}]$  do
13                             Retrieve the 45-bit  $\blacksquare$  of  $A^{(0)}$  and the two matching bits,
                                store the 45-bit  $\blacksquare$  in  $L_1$  indexed by the two matching bits
14                         end
15                         for  $2^2$  values of  $\blacksquare$  do
16                             Compute to the matching point (blue parts of (23)) and
                                store 2-bit  $\blacksquare$  of  $A^{(0)}$  in  $L_2$  indexed by the matching point
17                         end
18                         for values matched between  $L_1$  and  $L_2$  do
19                             Compute the first 2 Sboxes of  $S^{(3)}$ 
20                             if the 2 Sboxes satisfy the precomputed  $S_{\{*,0\}}^{(3)}$ 
21                                 /* probability of  $2^{-2}$ . This step is to avoid
                                    computing all Sboxes of  $S^{(3)}$  and only use
                                    partial Sboxes to filter first. */
22                                 then
23                                     if it leads to the given hash value then
24                                         Output the preimage
25                                     end
26                                 end
27                         end
28                     end
29                 end
30             end
31 end

```

- In Line 19, we need to compute the first two Sboxes of $A^{(3)}$, i.e., $5 \times 2 = 10$ bits. For the linear layer, each output bit depends on 3 input bits. Therefore, to compute the 10 bits of $A^{(3)}$, we have to know $10 \times 3 = 30$ bits of $S^{(2)}$, which are assumed to be involved in 30 Sboxes of $S^{(2)}$. Since in Line 9, the Sboxes determined by \blacksquare bits are already computed in round 0, we totally have to compute $47 + 64 + 30 + 2 = 143$ Sboxes to compute the first 2 Sboxes of $S^{(3)}$. The time of Line 19 is $2^{116-50+15+43+2} \times \frac{143}{2^{56}} = 2^{125.16}$ 4-round Ascon.
- In Line 23, the time is $2^{116-50+15+43+2-2} = 2^{124}$ 4-round Ascon.

The total time complexity is $2^{117} + 2^{79} + 2^{124.9} + 2^{118} + 2^{121.7} + 2^{125.16} + 2^{124} \approx 2^{126.4}$ 4-round Ascon. The memory is 2^{45} to store U . In addition, we also give a 3-round MitM preimage attack on Ascon-XOF in Supplementary Material E with time complexity of $2^{120.58}$ 3-round Ascon and memory complexity of 2^{39} . An experiment on the MitM episode is given in Supplementary Material F.

7 Conclusion

In this paper, we give the framework of the MitM attack on sponge-based hashing. To find good attacks, we build bit-level MILP based automatic tools for MitM attacks on Keccak-512, Ascon-XOF, and Xoodyak-XOF. Although the birthday-paradox MitM attack has been widely applied to block ciphers or MD-based hash functions since 1977, this is the first attempt to apply it to Keccak, etc. Our attacks lead to improved or first preimage attacks on reduced-round Keccak-512, Ascon-XOF, and Xoodyak-XOF.

Discussion. Similar to previous preimage attacks [34,44], our attack on Keccak also uses the linearization-based techniques. In previous linearization-based preimage attack [34,44], all the variables should not be multiplied with each other, so that one can build linear equations on those variables and the target bits. In our MitM attack, the variables are divided into two independent sets. Within each set, the variables can be multiplied with each other. However, any variable from one set should not be multiplied with the variables from the other set. For Keccak, to attack more rounds, we use a one-round linear structure to skip the MILP programming of the first round and accelerate the MILP model. It should be noted that the linear structure used in this paper is just a technique to accelerate the search. Moreover, by using the linear structure, the search only covers a small fraction of the whole space of the solutions, which may be not the optimal MitM attack at all. For other instances of Keccak, it is open problem to apply one or two-round linear structures in the search for MitM attacks.

References

1. Dor Amzaleg and Itai Dinur. Refined cryptanalysis of the GPRS ciphers GEA-1 and GEA-2. *IACR Cryptol. ePrint Arch.*, page 424, 2022.
2. Kazumaro Aoki and Yu Sasaki. Preimage attacks on one-block MD4, 63-step MD5 and more. In *SAC 2008*, volume 5381, pages 103–119. Springer, 2008.

- 783 3. Jean-Philippe Aumasson, Daniel J Bernstein, Ward Beullens, Christoph Dobrau-
784 nig, Maria Eichlseder, Scott Fluhrer, Stefan-Lukas Gazdag, Andreas Hülsing,
785 Panos Kampanakis, Stefan Kölbl, et al. SPHINCS+: Submission to the NIST
786 post-quantum project. 2019.
- 787 4. Jean-Philippe Aumasson, Willi Meier, and Florian Mendel. Preimage attacks on
788 3-pass HAVAL and step-reduced MD5. In *SAC 2008*, volume 5381, pages 120–135.
- 789 5. Zhenzhen Bao, Xiaoyang Dong, Jian Guo, Zheng Li, Danping Shi, Siwei Sun, and
790 Xiaoyun Wang. Automatic search of meet-in-the-middle preimage attacks on AES-
791 like hashing. In *EUROCRYPT 2021, Part I*, volume 12696, pages 771–804.
- 792 6. Zhenzhen Bao, Jian Guo, Danping Shi, and Yi Tu. Superposition meet-in-the-
793 middle attacks: Updates on fundamental security of AES-like hashing. Cryptology
794 ePrint Archive, Paper 2021/575, 2021. <https://eprint.iacr.org/2021/575>.
- 795 7. Christof Beierle, Patrick Derbez, Gregor Leander, Gaëtan Leurent, Håvard Rad-
796 dum, Yann Rotella, David Rupprecht, and Lukas Stennes. Cryptanalysis of the
797 GPRS encryption algorithms GEA-1 and GEA-2. In *EUROCRYPT 2021, Pro-
798 ceedings, Part II*, volume 12697, pages 155–183. Springer, 2021.
- 799 8. Daniel J. Bernstein. Second preimages for 6 (7?(8??)) rounds of Keccak. *NIST
800 mailing list*, 2010.
- 801 9. Guido Bertoni, Joan Daemen, Michaël Peeters, and Gilles Van Assche. Keccak
802 sponge function family main document. *Submission to NIST (Round 2)*, 3(30):320–
803 337, 2009.
- 804 10. Alex Biryukov, Patrick Derbez, and Léo Perrin. Differential analysis and meet-in-
805 the-middle attack against round-reduced TWINE. In *FSE 2015*, pages 3–27.
- 806 11. Andrey Bogdanov, Dmitry Khovratovich, and Christian Rechberger. Biclique
807 cryptanalysis of the full AES. In *ASIACRYPT 2011, Proceedings*, pages 344–371.
- 808 12. Andrey Bogdanov and Christian Rechberger. A 3-subset meet-in-the-middle at-
809 tack: Cryptanalysis of the lightweight block cipher KTANTAN. In *SAC 2010*,
810 volume 6544, pages 229–240. Springer, 2010.
- 811 13. Charles Bouillaguet, Patrick Derbez, and Pierre-Alain Fouque. Automatic search
812 of attacks on round-reduced AES and applications. In *CRYPTO 2011, Proceedings*,
813 volume 6841, pages 169–187. Springer, 2011.
- 814 14. Anne Canteaut, María Naya-Plasencia, and Bastien Vayssière. Sieve-in-the-middle:
815 Improved MITM attacks. In *CRYPTO 2013, Proceedings, Part I*, pages 222–240.
- 816 15. Joan Daemen, Seth Hoffert, Michaël Peeters, G Van Assche, and R Van Keer.
817 Xoodyak, a lightweight cryptographic scheme. 2020.
- 818 16. Ivan Damgård. A design principle for hash functions. In *CRYPTO ’89*, pages
819 416–427.
- 820 17. Hüseyin Demirci and Ali Aydin Selçuk. A meet-in-the-middle attack on 8-round
821 AES. In *FSE 2008*, pages 116–126. Springer, 2008.
- 822 18. Patrick Derbez and Pierre-Alain Fouque. Automatic search of meet-in-the-middle
823 and impossible differential attacks. In *CRYPTO 2016, Proceedings, Part II*, volume
824 9815, pages 157–184. Springer, 2016.
- 825 19. Patrick Derbez, Pierre-Alain Fouque, and Jérémy Jean. Improved key recovery
826 attacks on reduced-round AES in the single-key setting. In *EUROCRYPT 2013,
827 Proceedings*, volume 7881, pages 371–387. Springer, 2013.
- 828 20. Patrick Derbez and Léo Perrin. Meet-in-the-middle attacks and structural analysis
829 of round-reduced prince. In *FSE 2015*, pages 190–216. Springer, 2015.
- 830 21. Whitfield Diffie and Martin E. Hellman. Special feature exhaustive cryptanalysis
831 of the NBS data encryption standard. *Computer*, 10(6):74–84, 1977.

- 832 22. Itai Dinur. Cryptanalytic applications of the polynomial method for solving mul-
833 ti-variate equation systems over $\text{GF}(2)$. In *EUROCRYPT 2021, Proceedings, Part*
834 *I*, volume 12696, pages 374–403. Springer, 2021.
- 835 23. Itai Dinur, Orr Dunkelman, Nathan Keller, and Adi Shamir. Efficient dissection
836 of composite problems, with applications to cryptanalysis, knapsacks, and combi-
837 natorial search problems. In *CRYPTO 2012*, volume 7417, pages 719–740.
- 838 24. Itai Dinur, Orr Dunkelman, and Adi Shamir. Collision attacks on up to 5 rounds
839 of SHA-3 using generalized internal differentials. In *FSE 2013*, volume 8424, pages
840 219–240. Springer, 2013.
- 841 25. Itai Dinur and Adi Shamir. Breaking grain-128 with dynamic cube attacks. In
842 *FSE 2011*, volume 6733, pages 167–187. Springer, 2011.
- 843 26. Christoph Dobraunig, Maria Eichlseder, Florian Mendel, and Martin Schl  ffer. As-
844 con v1.2: Lightweight authenticated encryption and hashing. *J. Cryptol.*, 34(3):33,
845 2021.
- 846 27. Xiaoyang Dong, Jialiang Hua, Siwei Sun, Zheng Li, Xiaoyun Wang, and Lei Hu.
847 Meet-in-the-middle attacks revisited: Key-recovery, collision, and preimage attacks.
848 In *CRYPTO 2021, Proceedings, Part III*, volume 12827, pages 278–308. Springer.
- 849 28. Orr Dunkelman, Nathan Keller, and Adi Shamir. Improved single-key attacks on
850 8-round AES-192 and AES-256. In *ASIACRYPT 2010, Proceedings*, volume 6477,
851 pages 158–176. Springer, 2010.
- 852 29. Orr Dunkelman, Gautham Sekar, and Bart Preneel. Improved meet-in-the-middle
853 attacks on reduced-round DES. In *INDOCRYPT 2007, Proceedings*, volume 4859,
854 pages 86–100. Springer, 2007.
- 855 30. Thomas Espitau, Pierre-Alain Fouque, and Pierre Karpman. Higher-order differ-
856 ential meet-in-the-middle preimage attacks on SHA-1 and BLAKE. In *CRYPTO*
857 *2015, Proceedings, Part I*, volume 9215, pages 683–701. Springer, 2015.
- 858 31. Thomas Fuhr and Brice Minaud. Match box meet-in-the-middle attack against
859 KATAN. In *FSE 2014*, pages 61–81, 2014.
- 860 32. David G  rault, Thomas Peyrin, and Quan Quan Tan. Exploring differential-
861 based distinguishers and forgeries for ASCON. *IACR Trans. Symmetric Cryptol.*,
862 2021(3):102–136, 2021.
- 863 33. Jian Guo, San Ling, Christian Rechberger, and Huaxiong Wang. Advanced meet-
864 in-the-middle preimage attacks: First results on full Tiger, and improved results on
865 MD4 and SHA-2. In *ASIACRYPT 2010, Proceedings*, volume 6477, pages 56–75.
- 866 34. Jian Guo, Meicheng Liu, and Ling Song. Linear structures: Applications to crypt-
867 analysis of round-reduced Keccak. In *ASIACRYPT 2016, Proceedings, Part I*,
868 volume 10031, pages 249–274, 2016.
- 869 35. Le He, Xiaoen Lin, and Hongbo Yu. Improved preimage attacks on round-reduced
870 Keccak-384/512 via restricted linear structures. *Cryptol. ePrint Arch., Paper*,
871 2022/788.
- 872 36. Le He, Xiaoen Lin, and Hongbo Yu. Improved preimage attacks on 4-round Keccak-
873 224/256. *IACR Trans. Symmetric Cryptol.*, 2021(1):217–238, 2021.
- 874 37. Senyang Huang, Xiaoyun Wang, Guangwu Xu, Meiqin Wang, and Jingyuan Zhao.
875 Conditional cube attack on reduced-round Keccak sponge function. In *EURO-*
876 *CRYPT 2017, Proceedings, Part II*, volume 10211, pages 259–288, 2017.
- 877 38. Sebastiaan Indestege, Nathan Keller, Orr Dunkelman, Eli Biham, and Bart Pre-
878 neel. A practical attack on KeeLoq. In *EUROCRYPT 2008, Proceedings*, volume
879 4965, pages 1–18. Springer, 2008.
- 880 39. Takanori Isobe. A single-key attack on the full GOST block cipher. *J. Cryptol.*,
881 26(1):172–189, 2013.

- 882 40. Simon Knellwolf and Dmitry Khovratovich. New preimage attacks against reduced
883 SHA-1. In *CRYPTO 2012, Proceedings*, volume 7417, pages 367–383.
- 884 41. Simon Knellwolf, Willi Meier, and María Naya-Plasencia. Conditional differential
885 cryptanalysis of NLFSR-based cryptosystems. In *ASIACRYPT 2010 Proceedings*,
886 volume 6477, pages 130–145. Springer, 2010.
- 887 42. Stefan Kölbl, Martin M. Lauridsen, Florian Mendel, and Christian Rechberger.
888 Haraka v2 - efficient short-input hashing for post-quantum applications. *IACR*
889 *Trans. Symmetric Cryptol.*, 2016(2):1–29, 2016.
- 890 43. Gaëtan Leurent. MD4 is not one-way. In *FSE 2008*, volume 5086, pages 412–428.
- 891 44. Ting Li and Yao Sun. Preimage attacks on round-reduced Keccak-224/256 via an
892 allocating approach. In *EUROCRYPT 2019, Proceedings, Part III*, volume 11478,
893 pages 556–584. Springer, 2019.
- 894 45. Ting Li, Yao Sun, Maodong Liao, and Dingkan Wang. Preimage attacks on
895 the round-reduced Keccak with cross-linear structures. *IACR Trans. Symmetric*
896 *Cryptol.*, 2017(4):39–57, 2017.
- 897 46. Xiaoen Lin, Le He, and Hongbo Yu. Improved preimage attacks on 3-round Keccak-
898 224/256. *IACR Trans. Symmetric Cryptol.*, 2021(3):84–101, 2021.
- 899 47. Fukang Liu, Takanori Isobe, Willi Meier, and Zhonghao Yang. Algebraic attacks on
900 round-reduced Keccak. In *ACISP 2021, Proceedings*, volume 13083, pages 91–110.
- 901 48. Guozhen Liu, Jingwen Lu, Huina Li, Peng Tang, and Weidong Qiu. Preimage
902 attacks against lightweight scheme xoodoo based on deep learning. In *Future of*
903 *Information and Communication Conference*, pages 637–648. Springer, 2021.
- 904 49. Stefan Lucks. Attacking triple encryption. In *FSE '98, Proceedings*, volume 1372,
905 pages 239–253. Springer, 1998.
- 906 50. Ralph C. Merkle. A certified digital signature. In *CRYPTO 1989, Proceedings*,
907 pages 218–238, 1989.
- 908 51. Pawel Morawiecki, Josef Pieprzyk, and Marian Srebrny. Rotational cryptanalysis
909 of round-reduced Keccak. In *FSE 2013*, volume 8424, pages 241–262.
- 910 52. María Naya-Plasencia, Andrea Röck, and Willi Meier. Practical analysis of
911 reduced-round Keccak. In *INDOCRYPT 2011*, volume 7107, pages 236–254.
- 912 53. Bart Preneel, René Govaerts, and Joos Vandewalle. Hash functions based on block
913 ciphers: A synthetic approach. In *CRYPTO '93*, volume 773, pages 368–378.
- 914 54. Mahesh Sree Kumar Rajasree. Cryptanalysis of round-reduced Keccak using non-
915 linear structures. In *INDOCRYPT 2019*, volume 11898, pages 175–192.
- 916 55. Yu Sasaki. Integer linear programming for three-subset meet-in-the-middle attacks:
917 Application to GIFT. In *IWSEC 2018*, volume 11049, pages 227–243.
- 918 56. Yu Sasaki. Meet-in-the-middle preimage attacks on AES hashing modes and an
919 application to whirlpool. In *FSE 2011*, pages 378–396. Springer, 2011.
- 920 57. Yu Sasaki and Kazumaro Aoki. Finding preimages in full MD5 faster than exhaus-
921 tive search. In *EUROCRYPT 2009, Proceedings*, volume 5479, pages 134–152.
- 922 58. Yu Sasaki and Kazumaro Aoki. Preimage attacks on 3, 4, and 5-pass HAVAL. In
923 *ASIACRYPT 2008, Proceedings*, volume 5350, pages 253–271. Springer, 2008.
- 924 59. André Schrottenloher and Marc Stevens. Simplified MITM modeling for permuta-
925 tions: New (quantum) attacks. *IACR Cryptol. ePrint Arch.*, page 189, 2022.
- 926 60. Xiaoyun Wang, Yiqun Lisa Yin, and Hongbo Yu. Finding collisions in the full
927 SHA-1. In *CRYPTO 2005, Proceedings*, volume 3621, pages 17–36. Springer, 2005.
- 928 61. Xiaoyun Wang and Hongbo Yu. How to break MD5 and other hash functions. In
929 *EUROCRYPT 2005, Proceedings*, volume 3494, pages 19–35. Springer, 2005.

Supplementary Material

A An Example of the MitM Attack

We take the MitM preimage attack on 7-round AES-hashing in [56] as an example.

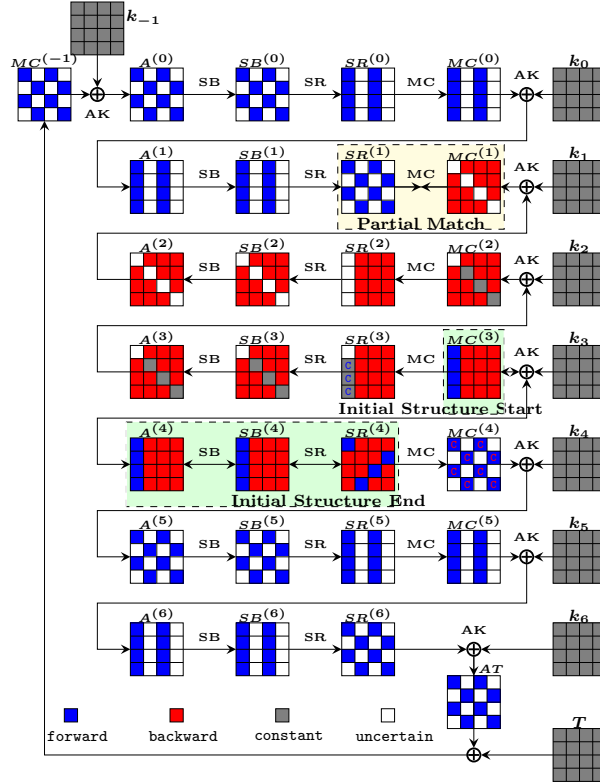


Fig. 15: The MitM preimage attack on 7-round AES-hashing.

Denote the internal states of round r as

$$A^{(r)} \xrightarrow{SB} SB^{(r)} \xrightarrow{SR} SR^{(r)} \xrightarrow{MC} MC^{(r)} \xrightarrow{AK} A^{(r+1)}.$$

$A_{\{i\}}^{(r)}$ represents the i -th ($0 \leq i \leq 15$) byte of state $A^{(r)}$ numbered from up to bottom, left to right. $A_{\{i-j\}}^{(r)}$ represents the i -th byte to j -th byte of state $A^{(r)}$.

Chunk Separation: As shown in Figure 15, the initial structure involves a few consecutive starting steps, i.e. $\{MC^{(3)}, A^{(4)}, SB^{(4)}, SR^{(4)}\}$. The $MC_{\{0-3\}}^{(3)}$

are chosen as neutral bytes (marked by blue) for the forward chunk and the $SR_{\{1-6,8,9,11,12,14,15\}}^{(4)}$ (marked by red) are chosen as neutral bytes for the backward chunk. Results from two chunks will match at $SR^{(1)}$ and $MC^{(1)}$ for a partial match.

Constraints on Initial Structure: To make the initial structure work, one needs to add 3 constraints on the neutral bytes for the forward chunk $MC_{\{0-3\}}^{(3)}$ to avoid the impacts on the backward chunk. The bytes $SR_{\{1,2,3\}}^{(3)}$ can be pre-determined constant values as follows:

$$\begin{cases} c_0 = 9 \cdot MC_{\{0\}}^{(3)} \oplus e \cdot MC_{\{1\}}^{(3)} \oplus b \cdot MC_{\{2\}}^{(3)} \oplus d \cdot MC_{\{3\}}^{(3)} \\ c_1 = d \cdot MC_{\{0\}}^{(3)} \oplus 9 \cdot MC_{\{1\}}^{(3)} \oplus e \cdot MC_{\{2\}}^{(3)} \oplus b \cdot MC_{\{3\}}^{(3)} \\ c_2 = b \cdot MC_{\{0\}}^{(3)} \oplus d \cdot MC_{\{1\}}^{(3)} \oplus 9 \cdot MC_{\{2\}}^{(3)} \oplus e \cdot MC_{\{3\}}^{(3)} \end{cases}. \quad (24)$$

There are 2^8 values of $MC_{\{0-3\}}^{(3)}$ when the constants c_0, c_1, c_2 are determined. Similarly, adding 8 constraints on the neutral bytes for the backward chunk to avoid the impacts on 8 bytes $MC_{\{0,2,5,7,8,10,13,15\}}^{(4)}$.

Matching through MC: According to the property of the MC operation, the match is tested column by column. There are totally five bytes known in each column of $SR^{(1)}$ and $MC^{(1)}$. So there has one byte matching for each column. Taking the match for first column as an example. The $SR_{\{0,2\}}^{(1)}$ are deduced in the forward computation and $MC_{\{1,2,3\}}^{(1)}$ are deduced in the backward computation. There has

$$\begin{aligned} & d \cdot SR_{\{0\}}^{(1)} \oplus e \cdot SR_{\{2\}}^{(1)} \\ = & d \cdot (b \cdot MC_{\{1\}}^{(1)} \oplus d \cdot MC_{\{2\}}^{(1)} \oplus 9 \cdot MC_{\{3\}}^{(1)}) \oplus e \cdot (9 \cdot MC_{\{1\}}^{(1)} \oplus e \cdot MC_{\{2\}}^{(1)} \oplus b \cdot MC_{\{3\}}^{(1)}). \end{aligned} \quad (25)$$

Forward and Backwork Computation: The forward computation list contains the blue neutral bits in $MC^{(3)}$ to $SR^{(1)}$. When accounting for the constraints, one can compute the neutral bytes in the forward chunk by traversing 2^8 possible values of $MC_{\{0-3\}}^{(3)}$. Then store $MC_{\{0-3\}}^{(3)}$ in table L_1 indexed by the value of $SR^{(1)}$ as the left part of Equ. (25) (i.e. $d \cdot SR_{\{0\}}^{(1)} \oplus e \cdot SR_{\{2\}}^{(1)}$). Similarly, the backward computation list contains the red neutral bits in $SR^{(4)}$ to $MC^{(1)}$. Store them in table L_2 indexed by the value of $MC^{(1)}$ as the right part of Equ. (25). Then one can use L_1 and L_2 for a 32-bit partial match on the indices.

964 B Figures of 4-round MitM Preimage Attack on 965 Keccak-512

The offset $\gamma[x, y]$ in Keccak round function is given in Table 4.

	$x = 0$	$x = 1$	$x = 2$	$x = 3$	$x = 4$
$y = 0$	0	1	62	28	27
$y = 1$	36	44	6	55	20
$y = 2$	3	10	43	25	39
$y = 3$	41	45	15	21	8
$y = 4$	18	2	61	56	14

Table 4: The offset $\gamma[x, y]$ in the ρ operation for Keccak

966 The figures of the 4-round MitM attack on Keccak-512 are given as Figure
967 10,16,17,18.
968

969 C An Experiment on 3-round Keccak-512

970 We give an experimental attack on 3-round Keccak-512 in Figure 19,20,21,22
971 to verify our method. In the attack, the starting state $A^{(0)}$ have 16 ■ and 16 ■
972 bits, which are given in Table 5. The consumes of degree of freedom happen at
973 the first θ operation due to the linear structure, which consuming 8 ■ and 8 ■.
974 Therefore, $\text{DoF}_B = 16 - 8 = 8$, $\text{DoF}_R = 16 - 8 = 8$. In Table 6, there are totally
975 64 conditions on $\theta^{(0)}$. The degree of matching is counted by the deterministic
976 relations of $A^{(2)}$ according to Observation 1, we get $\text{DoM} = 11$ and list the
977 equations for filtering as Equ. (26).

red bit	$A_{\{0,0,2\}}^{(0)}, A_{\{0,1,2\}}^{(0)}, A_{\{2,0,13\}}^{(0)}, A_{\{2,1,13\}}^{(0)}, A_{\{0,0,17\}}^{(0)}, A_{\{0,1,17\}}^{(0)}, A_{\{2,0,32\}}^{(0)}, A_{\{2,1,32\}}^{(0)},$ $A_{\{2,0,37\}}^{(0)}, A_{\{2,1,37\}}^{(0)}, A_{\{2,0,40\}}^{(0)}, A_{\{2,1,40\}}^{(0)}, A_{\{0,0,48\}}^{(0)}, A_{\{0,1,48\}}^{(0)}, A_{\{0,0,63\}}^{(0)}, A_{\{0,1,63\}}^{(0)}$
blue bit	$A_{\{0,0,8\}}^{(0)}, A_{\{0,1,8\}}^{(0)}, A_{\{0,0,9\}}^{(0)}, A_{\{0,1,9\}}^{(0)}, A_{\{0,0,13\}}^{(0)}, A_{\{0,1,13\}}^{(0)}, A_{\{0,0,41\}}^{(0)}, A_{\{0,1,41\}}^{(0)},$ $A_{\{2,0,45\}}^{(0)}, A_{\{2,1,45\}}^{(0)}, A_{\{2,0,49\}}^{(0)}, A_{\{2,1,49\}}^{(0)}, A_{\{2,0,62\}}^{(0)}, A_{\{2,1,62\}}^{(0)}, A_{\{2,0,1\}}^{(0)}, A_{\{2,1,1\}}^{(0)}$

Table 5: The red bits and blue bits in $A^{(0)}$ of 3-round experiment on Keccak-512

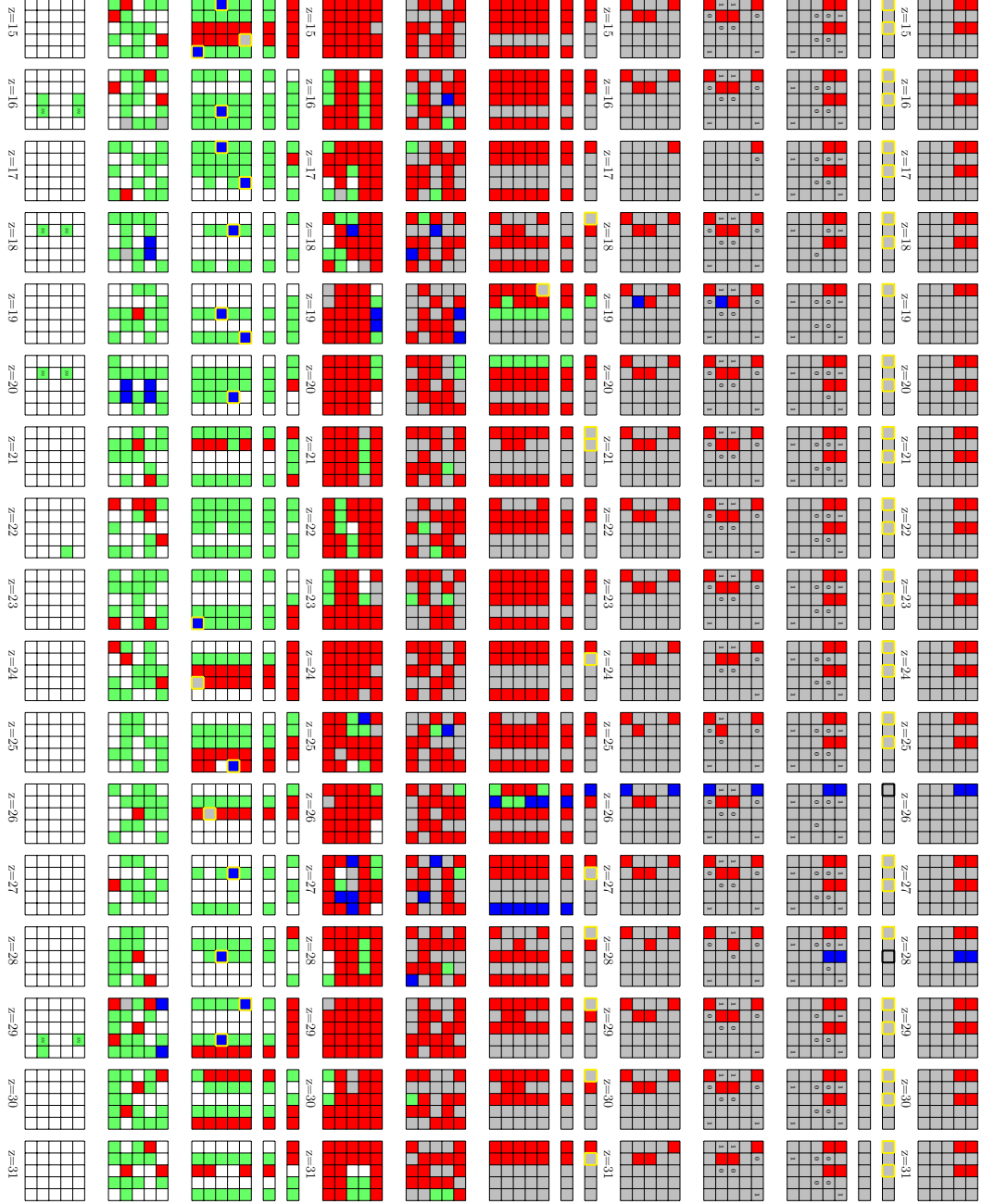


Fig. 16: The MitM preimage attack on 4-round Keccak-512 (part II)

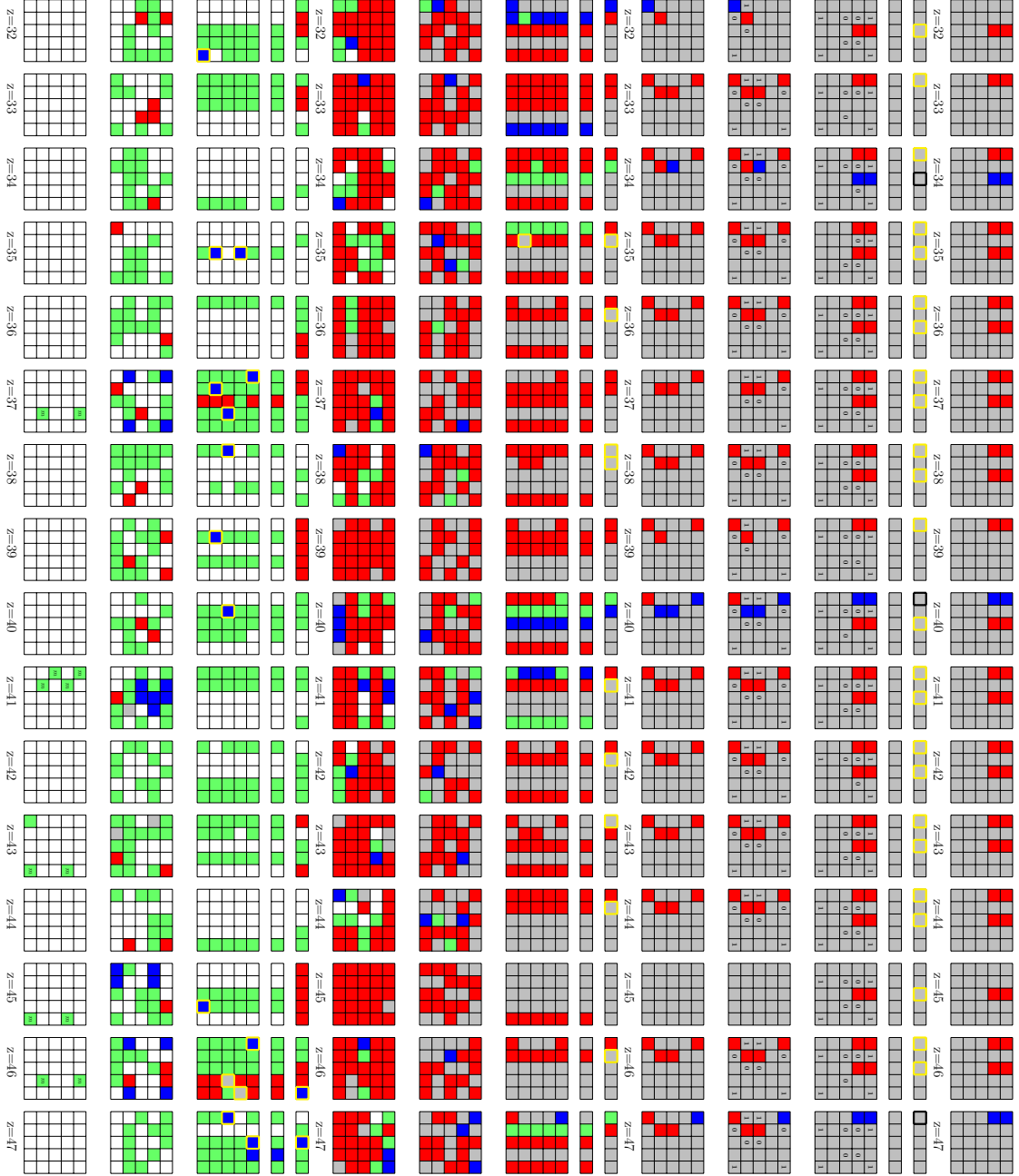


Fig. 17: The MitM preimage attack on 4-round Keccak-512 (part III)

Fig. 18: The MitM preimage attack on 4-round Keccak-512 (part IV)

$$\begin{aligned}
&\theta_{\{1,1,4\}}^{(0)} = 0, \theta_{\{1,1,19\}}^{(0)} = 0, \theta_{\{1,1,22\}}^{(0)} = 0, \theta_{\{1,1,28\}}^{(0)} = 0, \theta_{\{1,1,29\}}^{(0)} = 0, \theta_{\{1,1,33\}}^{(0)} = 0, \\
&\theta_{\{1,1,37\}}^{(0)} = 0, \theta_{\{1,1,61\}}^{(0)} = 0, \theta_{\{1,2,3\}}^{(0)} = 0, \theta_{\{1,2,10\}}^{(0)} = 0, \theta_{\{1,2,25\}}^{(0)} = 0, \theta_{\{1,2,28\}}^{(0)} = 0, \\
&\theta_{\{1,2,34\}}^{(0)} = 0, \theta_{\{1,2,35\}}^{(0)} = 0, \theta_{\{1,2,39\}}^{(0)} = 0, \theta_{\{1,2,43\}}^{(0)} = 0, \theta_{\{3,1,5\}}^{(0)} = 0, \theta_{\{3,1,8\}}^{(0)} = 0, \\
&\theta_{\{3,1,20\}}^{(0)} = 0, \theta_{\{3,1,39\}}^{(0)} = 0, \theta_{\{3,1,44\}}^{(0)} = 0, \theta_{\{3,1,47\}}^{(0)} = 0, \theta_{\{3,1,52\}}^{(0)} = 0, \theta_{\{3,1,56\}}^{(0)} = 0, \\
&\theta_{\{3,2,13\}}^{(0)} = 0, \theta_{\{3,2,18\}}^{(0)} = 0, \theta_{\{3,2,21\}}^{(0)} = 0, \theta_{\{3,2,26\}}^{(0)} = 0, \theta_{\{3,2,30\}}^{(0)} = 0, \theta_{\{3,2,43\}}^{(0)} = 0, \\
&\theta_{\{3,2,46\}}^{(0)} = 0, \theta_{\{3,2,58\}}^{(0)} = 0,
\end{aligned}$$

$$\begin{aligned}
&\theta_{\{1,0,3\}}^{(0)} = 1, \theta_{\{1,0,6\}}^{(0)} = 1, \theta_{\{1,0,18\}}^{(0)} = 1, \theta_{\{1,0,37\}}^{(0)} = 1, \theta_{\{1,0,42\}}^{(0)} = 1, \theta_{\{1,0,45\}}^{(0)} = 1, \\
&\theta_{\{1,0,50\}}^{(0)} = 1, \theta_{\{1,0,54\}}^{(0)} = 1, \theta_{\{1,4,9\}}^{(0)} = 1, \theta_{\{1,4,28\}}^{(0)} = 1, \theta_{\{1,4,33\}}^{(0)} = 1, \theta_{\{1,4,36\}}^{(0)} = 1, \\
&\theta_{\{1,4,41\}}^{(0)} = 1, \theta_{\{1,4,45\}}^{(0)} = 1, \theta_{\{1,4,58\}}^{(0)} = 1, \theta_{\{1,4,61\}}^{(0)} = 1, \theta_{\{4,0,8\}}^{(0)} = 1, \theta_{\{4,0,11\}}^{(0)} = 1, \\
&\theta_{\{4,0,17\}}^{(0)} = 1, \theta_{\{4,0,18\}}^{(0)} = 1, \theta_{\{4,0,22\}}^{(0)} = 1, \theta_{\{4,0,26\}}^{(0)} = 1, \theta_{\{4,0,50\}}^{(0)} = 1, \theta_{\{4,0,57\}}^{(0)} = 1, \\
&\theta_{\{4,4,3\}}^{(0)} = 1, \theta_{\{4,4,27\}}^{(0)} = 1, \theta_{\{4,4,34\}}^{(0)} = 1, \theta_{\{4,4,49\}}^{(0)} = 1, \theta_{\{4,4,52\}}^{(0)} = 1, \theta_{\{4,4,58\}}^{(0)} = 1, \\
&\theta_{\{4,4,59\}}^{(0)} = 1, \theta_{\{4,4,63\}}^{(0)} = 1.
\end{aligned}$$

Table 6: Bit conditions in $\theta^{(0)}$ of 3-round experiment on Keccak-512

$$\begin{aligned}
&A_{\{3,0,36\}}^{(2)} \oplus A_{\{3,3,36\}}^{(2)} \oplus (A_{\{1,1,0\}}^{(3)} \oplus 1) \cdot (A_{\{0,2,61\}}^{(2)} \oplus A_{\{0,0,61\}}^{(2)}) \oplus A_{\{0,1,0\}}^{(3)} \oplus \theta_{\{3,3,36\}}^{(3)} \oplus (A_{\{1,1,0\}}^{(3)} \oplus 1) \cdot \theta_{\{0,0,61\}}^{(2)} = 0, \\
&A_{\{3,0,58\}}^{(2)} \oplus A_{\{3,3,58\}}^{(2)} \oplus (A_{\{1,1,22\}}^{(3)} \oplus 1) \cdot (A_{\{0,2,19\}}^{(2)} \oplus A_{\{0,0,19\}}^{(2)}) \oplus A_{\{0,1,22\}}^{(3)} \oplus \theta_{\{3,3,58\}}^{(3)} \oplus (A_{\{1,1,22\}}^{(3)} \oplus 1) \cdot \theta_{\{0,0,19\}}^{(2)} = 0, \\
&A_{\{3,0,2\}}^{(2)} \oplus A_{\{3,3,2\}}^{(2)} \oplus (A_{\{1,1,30\}}^{(3)} \oplus 1) \cdot (A_{\{0,2,27\}}^{(2)} \oplus A_{\{0,0,27\}}^{(2)}) \oplus A_{\{0,1,30\}}^{(3)} \oplus \theta_{\{3,3,2\}}^{(3)} \oplus (A_{\{1,1,30\}}^{(3)} \oplus 1) \cdot \theta_{\{0,0,27\}}^{(2)} = 0, \\
&A_{\{3,0,27\}}^{(2)} \oplus A_{\{3,3,27\}}^{(2)} \oplus (A_{\{1,1,55\}}^{(3)} \oplus 1) \cdot (A_{\{0,2,52\}}^{(2)} \oplus A_{\{0,0,52\}}^{(2)}) \oplus A_{\{0,1,55\}}^{(3)} \oplus \theta_{\{3,3,27\}}^{(3)} \oplus (A_{\{1,1,55\}}^{(3)} \oplus 1) \cdot \theta_{\{0,0,52\}}^{(2)} = 0, \\
&A_{\{4,1,1\}}^{(2)} \oplus A_{\{4,4,1\}}^{(2)} \oplus (A_{\{2,1,21\}}^{(3)} \oplus 1) \cdot (A_{\{1,3,40\}}^{(2)} \oplus A_{\{1,1,40\}}^{(2)}) \oplus A_{\{1,1,21\}}^{(3)} \oplus \theta_{\{4,4,1\}}^{(3)} \oplus (A_{\{2,1,21\}}^{(3)} \oplus 1) \cdot \theta_{\{1,1,40\}}^{(2)} = 0, \\
&A_{\{4,1,4\}}^{(2)} \oplus A_{\{4,4,4\}}^{(2)} \oplus (A_{\{2,1,24\}}^{(3)} \oplus 1) \cdot (A_{\{1,3,43\}}^{(2)} \oplus A_{\{1,1,43\}}^{(2)}) \oplus A_{\{1,1,24\}}^{(3)} \oplus \theta_{\{4,4,4\}}^{(3)} \oplus (A_{\{2,1,24\}}^{(3)} \oplus 1) \cdot \theta_{\{1,1,43\}}^{(2)} = 0, \\
&A_{\{4,1,5\}}^{(2)} \oplus A_{\{4,4,5\}}^{(2)} \oplus (A_{\{2,1,25\}}^{(3)} \oplus 1) \cdot (A_{\{1,3,44\}}^{(2)} \oplus A_{\{1,1,44\}}^{(2)}) \oplus A_{\{1,1,25\}}^{(3)} \oplus \theta_{\{4,4,5\}}^{(3)} \oplus (A_{\{2,1,25\}}^{(3)} \oplus 1) \cdot \theta_{\{1,1,44\}}^{(2)} = 0, \\
&A_{\{4,1,17\}}^{(2)} \oplus A_{\{4,4,17\}}^{(2)} \oplus (A_{\{2,1,37\}}^{(3)} \oplus 1) \cdot (A_{\{1,3,56\}}^{(2)} \oplus A_{\{1,1,56\}}^{(2)}) \oplus A_{\{1,1,37\}}^{(3)} \oplus \theta_{\{4,4,17\}}^{(3)} \oplus (A_{\{2,1,37\}}^{(3)} \oplus 1) \cdot \theta_{\{1,1,56\}}^{(2)} = 0, \\
&A_{\{4,1,20\}}^{(2)} \oplus A_{\{4,4,20\}}^{(2)} \oplus (A_{\{2,1,40\}}^{(3)} \oplus 1) \cdot (A_{\{1,3,59\}}^{(2)} \oplus A_{\{1,1,59\}}^{(2)}) \oplus A_{\{1,1,40\}}^{(3)} \oplus \theta_{\{4,4,20\}}^{(3)} \oplus (A_{\{2,1,40\}}^{(3)} \oplus 1) \cdot \theta_{\{1,1,59\}}^{(2)} = 0, \\
&A_{\{4,1,41\}}^{(2)} \oplus A_{\{4,4,41\}}^{(2)} \oplus (A_{\{2,1,61\}}^{(3)} \oplus 1) \cdot (A_{\{1,3,16\}}^{(2)} \oplus A_{\{1,1,16\}}^{(2)}) \oplus A_{\{1,1,61\}}^{(3)} \oplus \theta_{\{4,4,41\}}^{(3)} \oplus (A_{\{2,1,61\}}^{(3)} \oplus 1) \cdot \theta_{\{1,1,16\}}^{(2)} = 0, \\
&A_{\{4,1,43\}}^{(2)} \oplus A_{\{4,4,43\}}^{(2)} \oplus (A_{\{2,1,63\}}^{(3)} \oplus 1) \cdot (A_{\{1,3,18\}}^{(2)} \oplus A_{\{1,1,18\}}^{(2)}) \oplus A_{\{1,1,63\}}^{(3)} \oplus \theta_{\{4,4,43\}}^{(3)} \oplus (A_{\{2,1,63\}}^{(3)} \oplus 1) \cdot \theta_{\{1,1,18\}}^{(2)} = 0.
\end{aligned}$$

(26)

978 **Experiments.** We use two message blocks (M_1, M_2) to conduct the MitM
979 experiment on 3-round Keccak-512. For message block M_2 , we randomly choose
980 its values, and set $A_{\{0,0,z\}} = A_{\{0,1,z\}}$ and $A_{\{2,0,z\}} = A_{\{2,1,z\}}$ for the ■ and ■ bits
981 listed in Table 5 due to the linear structure. To make the experiment simple,
982 we carefully set the inner part to make the 64 bit conditions in Table 6 satisfied
983 directly, and only test the MitM episodes. We pre-compute the hash value as
984 the target. We only test one MitM episode, where the other bits exclude ■ and ■
985 bits in $A^{(0)}$ keep unchanged with the above settings. Similar with Algorithm 1,
986 $2^8 \times 2^8$ values of ■ and ■ bits are exhausted and filtered with Equ. (26) in
987 the episode. We make the experiment for 10 times with different M_2 and pre-
988 computed targets, and the right values for ■ and ■ bits will remain among the

989 $2^8 \times 2^8 \times 2^{-11} = 2^5$ matched states. The details of the code are provided at <https://anonymous.4open.science/r/Conditional-MITM-Preimage-Attack>.
 990

991 D The Attack Algorithm of 3-round Xoodyak-XOF

992 By our MILP model, we derive the MitM characteristic on 3-round Xoodyak-XOF
 993 in Figure 23. The 3-round attack on Xoodyak-XOF is given in Algorithm 3.

994 E MitM Preimage Attack on Round-Reduced Ascon-XOF

995 E.1 Figures of 4-round Attack on Ascon-XOF

996 Solving our MILP model for Ascon, we get a 4-round MITM preimage attack as
 997 shown in Figure 24.

998 E.2 3-round Attack on Ascon-XOF

999 We follow similar framework in Figure 6 and perform the attack with three
 1000 message blocks (M_1, M_2, M_3) , where M_3 has two padding bits ‘10’. The MITM
 1001 attack is placed in the 3rd block. Solving with our MILP model for Ascon, we
 1002 get a 3-round MITM preimage attack as shown in Figure 25. The starting state
 1003 $A^{(0)}$ contains 10 ■ bits and 39 ■ bits. There are totally 54 conditions on ■ bits
 1004 of $A^{(0)}$, which are listed in Table 7. In the computation from $A^{(0)}$ to $A^{(2)}$, the
 1005 accumulated consumed degree of freedom of ■ is 29 and there is no DoF of ■
 1006 consumed. Therefore, $\text{DoF}_B = 10$, $\text{DoF}_R = 39 - 29 = 10$. The degree of matching
 1007 is counted by the deterministic relations of $A^{(2)}$ according to Observation 3, we
 1008 get $\text{DoM} = 10$.

1009 Before the MITM attack, we need to find a right (M_1, M_2) to make the
 1010 54 conditions in Table 7 hold with probability of 2^{-54} . Once we find a right
 1011 (M_1, M_2) , we search the space of M_3 with MITM method to find the preimage,
 1012 whose size is 2^{62} (there are 2 padding bits fixed). Therefore, to find a 128-bit
 1013 target preimage, we need $2^{128-62} = 2^{66}$ right (M_1, M_2) , which need $2^{66+54} =$
 1014 2^{120} time complexity to find. Then we call Algorithm 4 to perform the MITM
 1015 preimage attack on the 3-round Ascon. In Line 7, the time complexity is $2^{120} \times$
 1016 $2^{-54} \times 2^{13} \times 2^{39} = 2^{118}$. The time of one MITM episode between Line 9 to 17 is
 1017 about 2^{10} 3-round Ascon. The total time is $2^{120} + 2^{118} + 2^{120-54+13+29} \times 2^{10} =$
 1018 $2^{120.58}$. The memory to store U is 2^{39} .

1019 F An Experiment on 3-round Ascon-XOF

1020 We give an experimental test of the MITM episode on 3-round Ascon-XOF in
 1021 Figure 26 to verify our method. In the attack, the starting state $A^{(0)}$ have 7 ■
 1022 and 5 ■ bits. The consumes of degree of freedom happen at the second linear
 1023 layer, which consuming 2 ■. Therefore, $\text{DoF}_B = 5$, $\text{DoF}_R = 7 - 2 = 5$. In Table 8,

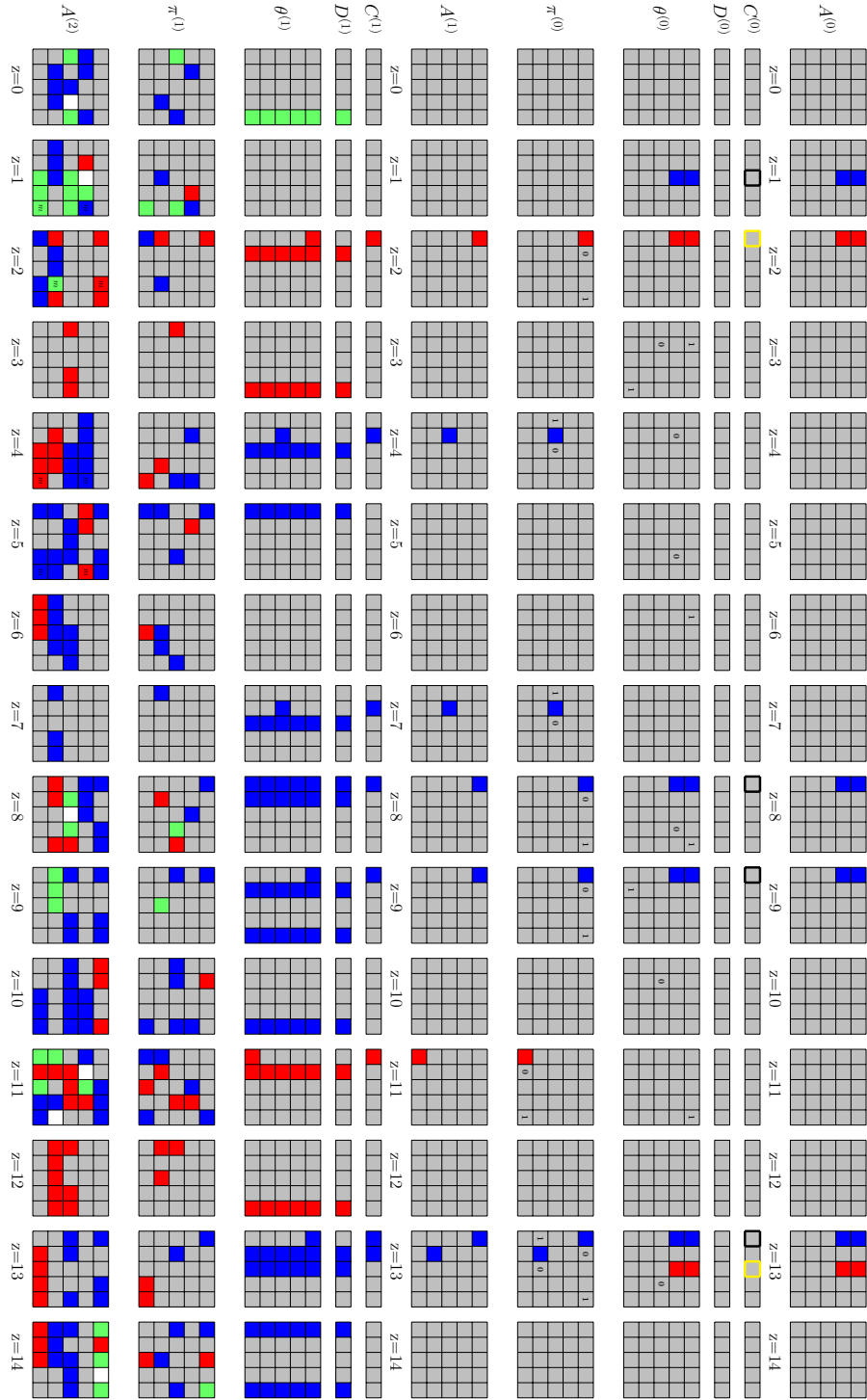


Fig. 19: The 3-round experiment on Keccak-512 (Part I)

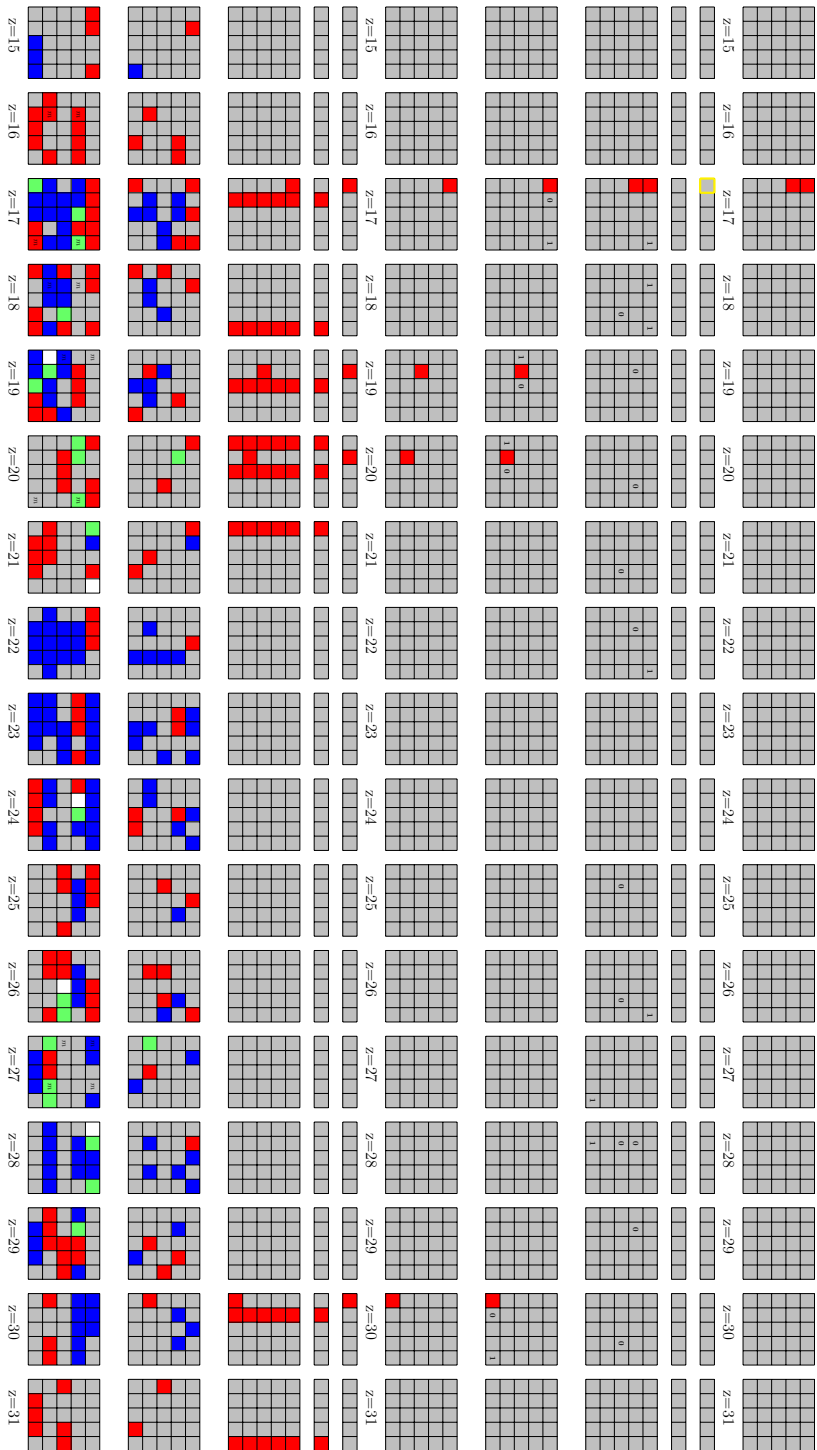


Fig. 20: The 3-round experiment on Keccak-512 (Part II)

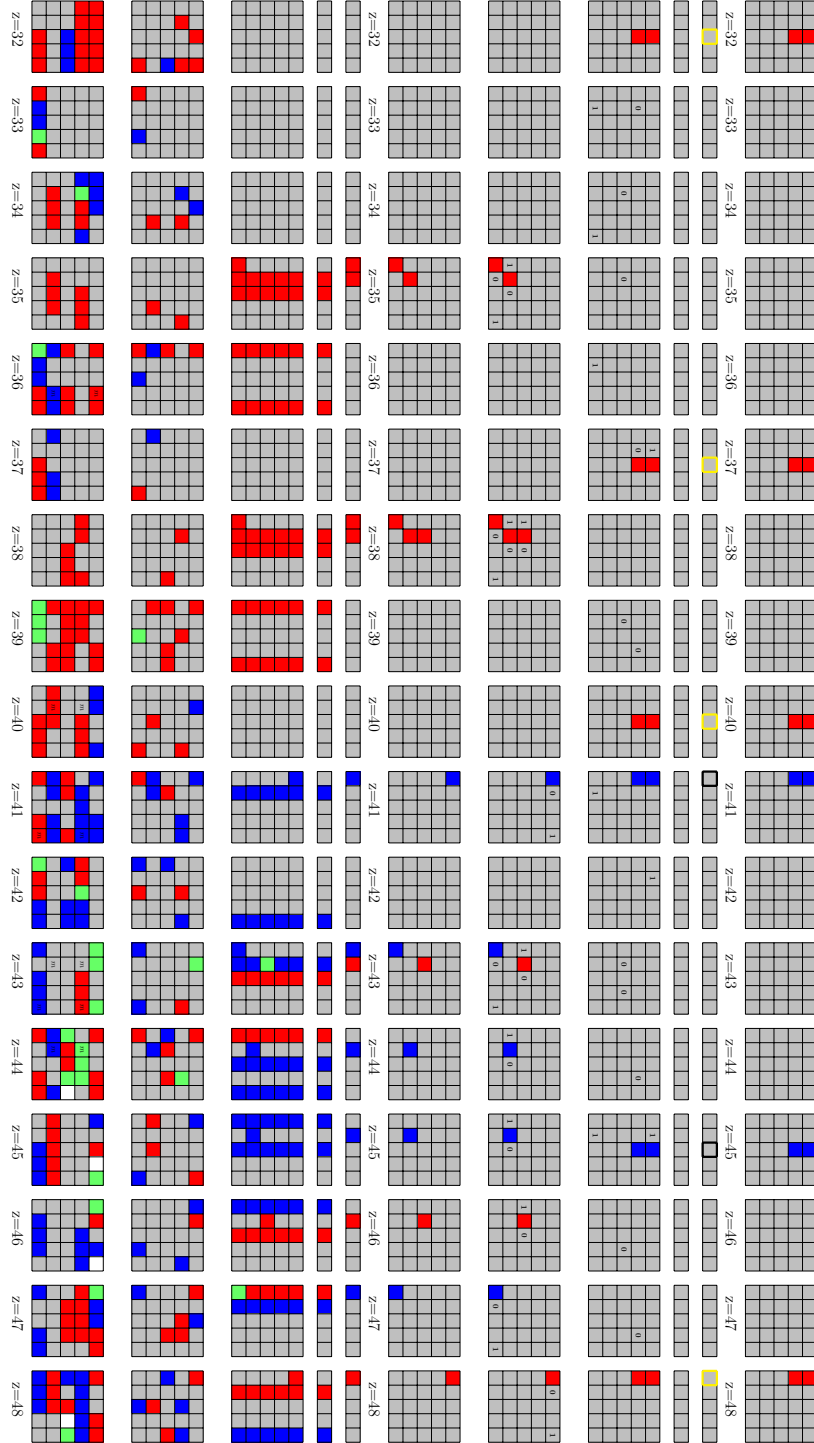


Fig. 21: The 3-round experiment on Keccak-512 (Part III)

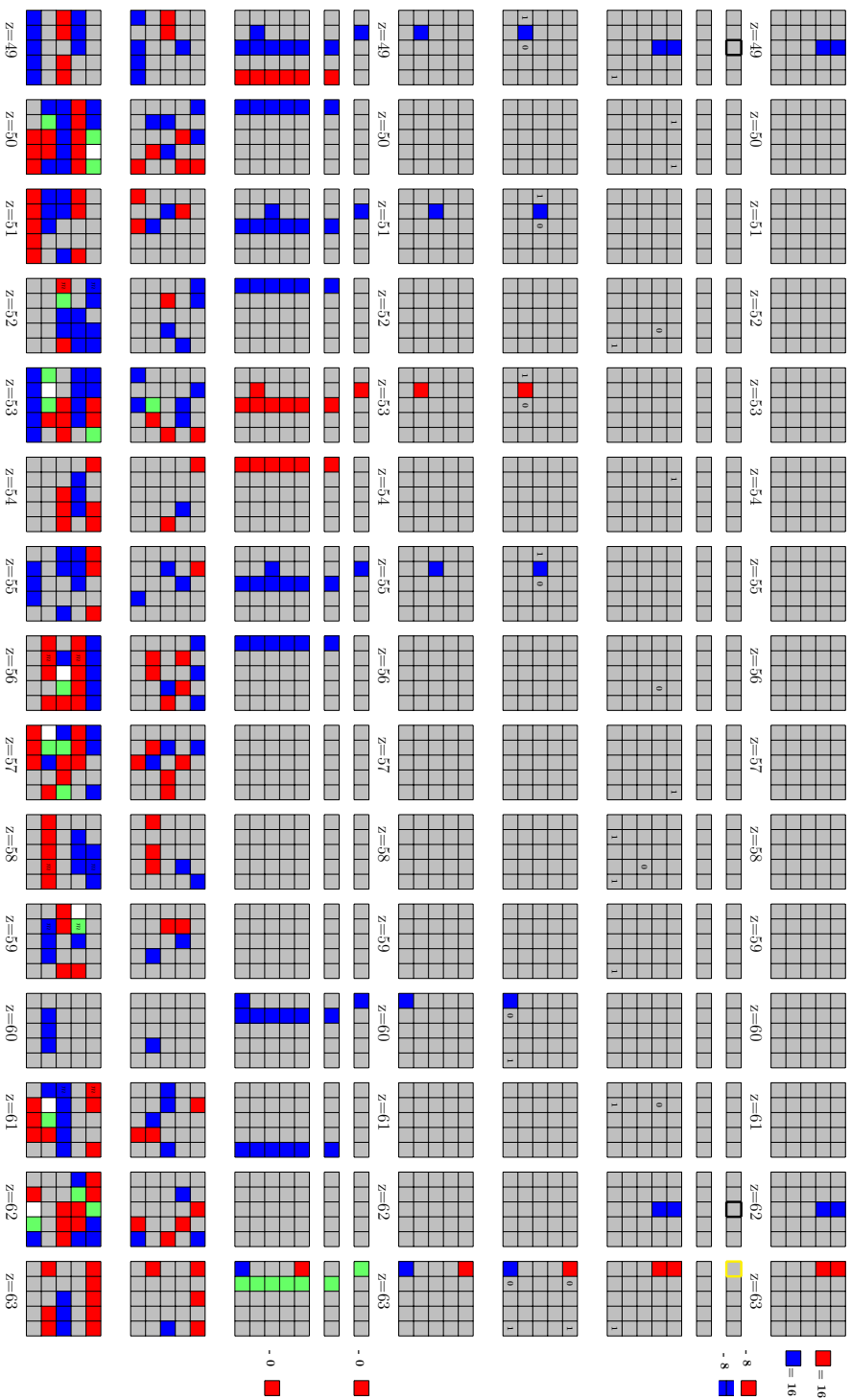


Fig. 22: The 3-round experiment on Keccak-512 (Part IV)

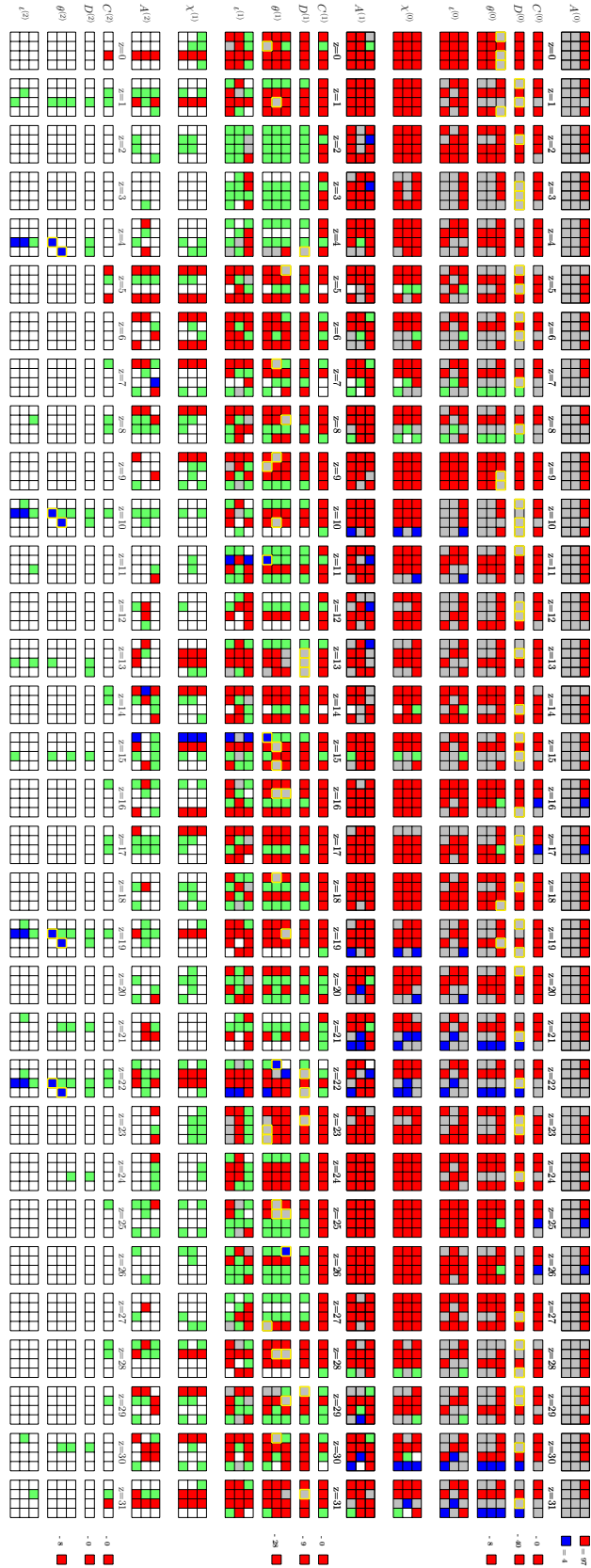


Fig. 23: The mitm preimage attack on 3-round Xoodyak-XOF

Algorithm 3: Preimage Attack on 3-round Xoodyak-XOF

```

1 for  $2^x$  values of  $M_1$  do
2   Compute the inner part of the 2nd block and solve the system of 53 linear
   equations
3   if the equations have solutions /* with probability of  $2^{-40}$  */
4   then
5     for each of the  $2^{12}$  solutions of  $M_2$  do
6       /* With  $x = 55$ , there are  $2^{55-40+12} = 2^{27}$  iterations */
7       Traversing the  $2^{97}$  values of  $\blacksquare$  in  $A^{(0)}$  while fixing  $\blacksquare$  as 0, compute
       forward to determine 93-bit  $\blacksquare/\blacksquare$  bits (denoted as  $c_{\mathcal{R}} \in \mathbb{F}_2^{93}$ ), and
       the 4-bit matching point in Equ. (22), i.e., compute four bits
        $f'_{\mathcal{M}} = f_{\mathcal{R}} \oplus f_{\mathcal{G}}$ . Build the table  $U$  and store the 97-bit  $\blacksquare$  bits of
        $A^{(0)}$  as well as the 4-bit matching point in  $U[c_{\mathcal{R}}]$ .
8       for  $c_{\mathcal{R}} \in \mathbb{F}_2^{93}$  do
9         Randomly pick a 97-bit  $\blacksquare e \in U[c_{\mathcal{R}}]$ , and set  $\blacksquare$  in  $A^{(0)}$  as 0,
         compute to the matching point to get 4 bits
          $f'''_{\mathcal{M}} = f_{\mathcal{G}} + \text{Const}(e)$ 
10        for  $2^4$  values in  $U[c_{\mathcal{R}}]$  do
11          Restore the values of  $\blacksquare$  of  $A^{(0)}$  and the corresponding
          matching point (i.e.,  $4 f_{\mathcal{R}} \oplus f_{\mathcal{G}} = f'_{\mathcal{M}}$ ) in a list  $L_1$ 
          (indexed by matching point)
12        end
13        for  $2^4$  values of  $\blacksquare$  do
14          Set the 97-bit  $\blacksquare$  in  $A^{(1)}$  as  $e$ . Compute to the matching
          point to get eight  $f''_{\mathcal{M}} = f_{\mathcal{B}} + f_{\mathcal{G}} + \text{Const}(e)$ . Together
          with  $f'''_{\mathcal{M}}$ , compute  $f_{\mathcal{B}} = f''_{\mathcal{M}} + f'''_{\mathcal{M}}$  and store  $\blacksquare$  in  $L_2$ 
          indexed by matching point.
15        end
16        for values matched between  $L_1$  and  $L_2$  do
17          Compute  $\iota^{(2)}$  from the matched  $\blacksquare$  and  $\blacksquare$  cells
18          if  $\iota^{(2)}$  satisfy the first 5 Sbox /* Probability of  $2^{-5}$ .
          This step is to avoid computing all Sboxes of
           $\iota^{(2)}$  and only use partial Sboxes to filter first.
          */
19          then
20            Check  $\iota^{(2)}$  against the remaining 119 Sboxes
21            if it leads to the given hash value then
22              Output the preimage
23            end
24          end
25        end
26      end
27    end
28  end
29 end

```

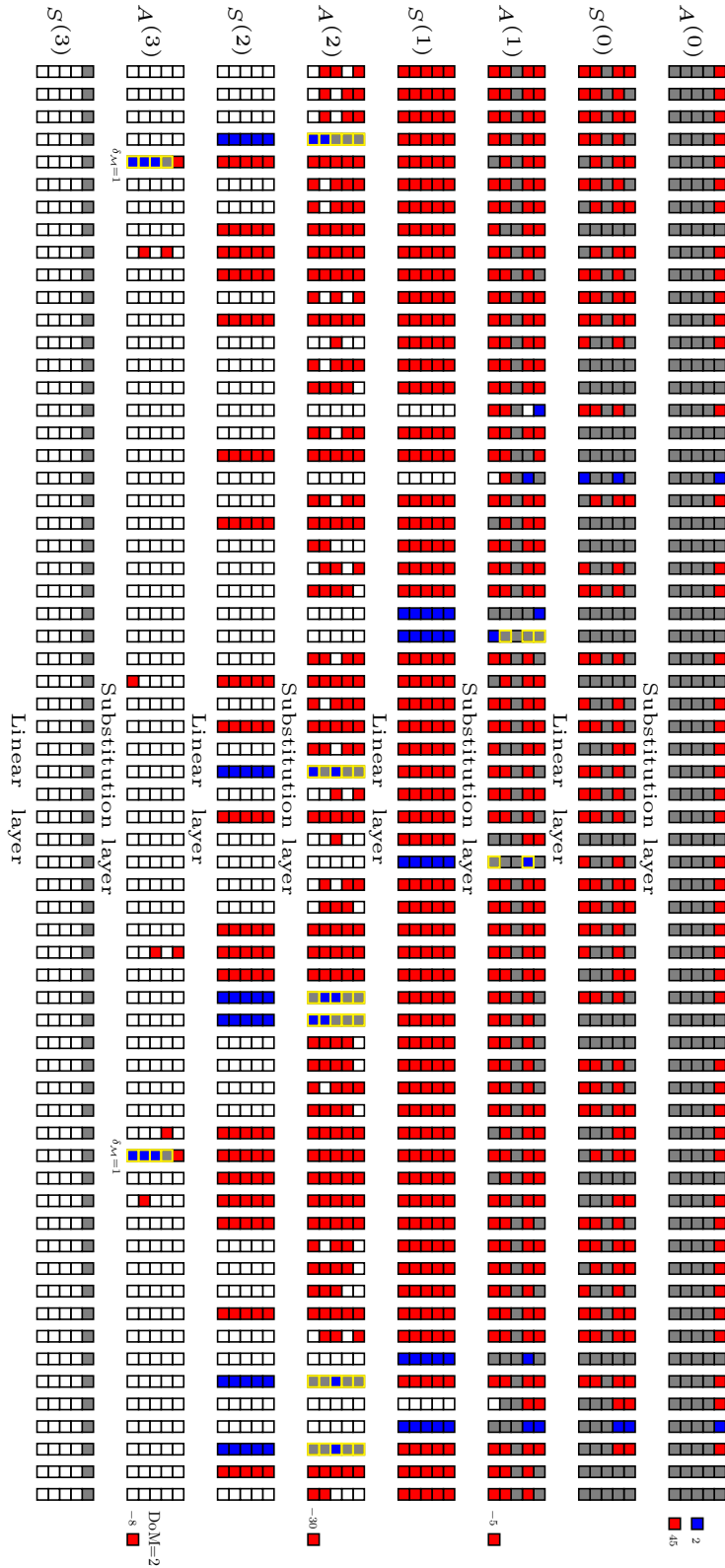


Fig. 24: The MITM preimage attack on 4-round Ascon-XOF

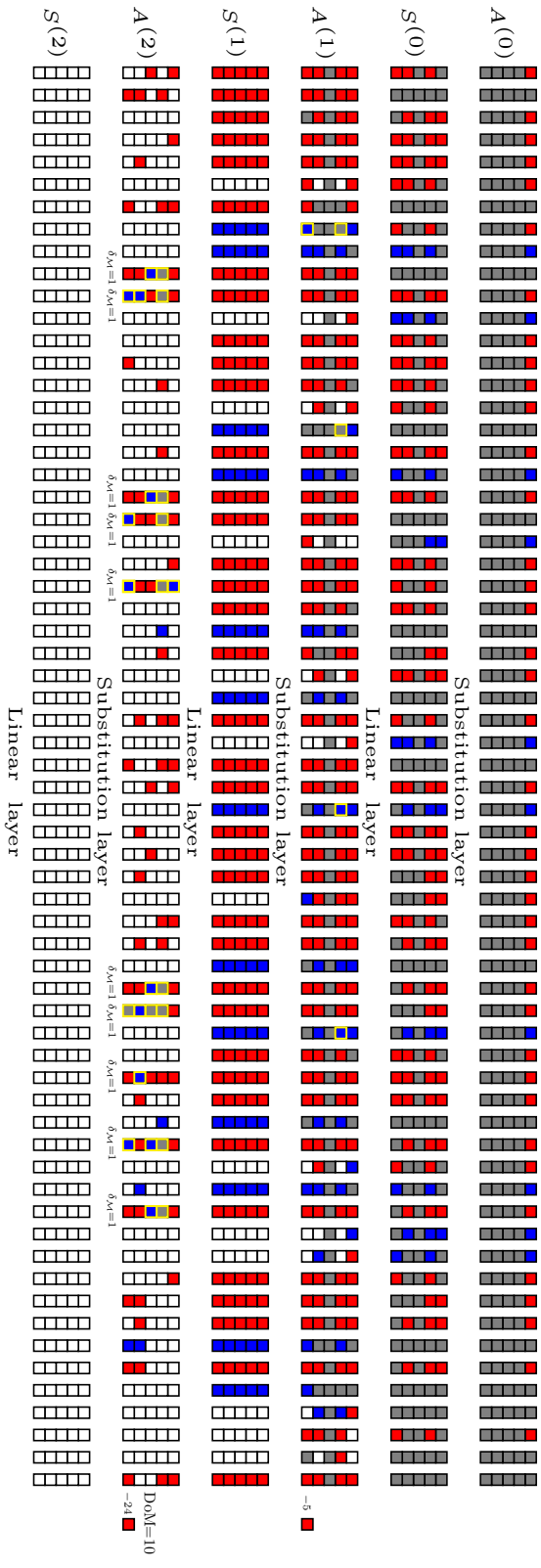


Fig. 25: The MitM preimage attack on 3-round Ascon-XOF

$A_{\{0,1\}}^{(0)} = 1; A_{\{2,1\}}^{(0)} = 0; A_{\{5,1\}}^{(0)} = 1; A_{\{7,1\}}^{(0)} = 1, A_{\{7,3\}}^{(0)} \oplus A_{\{7,4\}}^{(0)} = 1; A_{\{8,1\}}^{(0)} = 1;$
$A_{\{11,1\}}^{(0)} = 1; A_{\{12,1\}}^{(0)} = 1; A_{\{14,1\}}^{(0)} = 1; A_{\{15,1\}}^{(0)} = 1, A_{\{15,3\}}^{(0)} \oplus A_{\{15,4\}}^{(0)} = 1;$
$A_{\{18,1\}}^{(0)} = 1, A_{\{18,3\}}^{(0)} \oplus A_{\{18,4\}}^{(0)} = 1; A_{\{19,1\}}^{(0)} = 1; A_{\{21,1\}}^{(0)} = 0, A_{\{21,3\}}^{(0)} \oplus A_{\{21,4\}}^{(0)} = 1;$
$A_{\{22,1\}}^{(0)} = 1; A_{\{23,1\}}^{(0)} = 1, A_{\{23,3\}}^{(0)} \oplus A_{\{23,4\}}^{(0)} = 1; A_{\{24,1\}}^{(0)} = 1;$
$A_{\{26,1\}}^{(0)} = 0, A_{\{26,3\}}^{(0)} \oplus A_{\{26,4\}}^{(0)} = 1; A_{\{29,1\}}^{(0)} = 1, A_{\{29,3\}}^{(0)} \oplus A_{\{29,4\}}^{(0)} = 1; A_{\{30,1\}}^{(0)} = 1;$
$A_{\{33,1\}}^{(0)} = 0; A_{\{36,1\}}^{(0)} = 0, A_{\{36,3\}}^{(0)} \oplus A_{\{36,4\}}^{(0)} = 1; A_{\{37,1\}}^{(0)} = 0, A_{\{37,3\}}^{(0)} \oplus A_{\{37,4\}}^{(0)} = 1;$
$A_{\{38,1\}}^{(0)} = 1; A_{\{39,1\}}^{(0)} = 0; A_{\{41,1\}}^{(0)} = 0; A_{\{42,1\}}^{(0)} = 0, A_{\{42,3\}}^{(0)} \oplus A_{\{42,4\}}^{(0)} = 1; A_{\{43,1\}}^{(0)} = 0;$
$A_{\{44,1\}}^{(0)} = 1; A_{\{48,1\}}^{(0)} = 0; A_{\{49,1\}}^{(0)} = 1, A_{\{49,3\}}^{(0)} \oplus A_{\{49,4\}}^{(0)} = 1;$
$A_{\{50,1\}}^{(0)} = 1, A_{\{50,3\}}^{(0)} \oplus A_{\{50,4\}}^{(0)} = 1; A_{\{51,1\}}^{(0)} = 0; A_{\{52,1\}}^{(0)} = 0;$
$A_{\{53,1\}}^{(0)} = 1, A_{\{53,3\}}^{(0)} \oplus A_{\{53,4\}}^{(0)} = 1; A_{\{54,1\}}^{(0)} = 1, A_{\{54,3\}}^{(0)} \oplus A_{\{54,4\}}^{(0)} = 1;$
$A_{\{55,1\}}^{(0)} = 0, A_{\{55,3\}}^{(0)} \oplus A_{\{55,4\}}^{(0)} = 1; A_{\{56,1\}}^{(0)} = 0; A_{\{58,1\}}^{(0)} = 0;$
$A_{\{61,1\}}^{(0)} = 1, A_{\{61,3\}}^{(0)} \oplus A_{\{61,4\}}^{(0)} = 1$

Table 7: Bit Conditions in 3-round Attack on Ascon-XOF

Algorithm 4: Preimage Attack on 3-round Ascon-XOF

```

1 for  $2^{120}$  values of  $(M_1, M_2)$  do
2   Compute the inner part of the 3rd block
3   if the conditions of Table 7 are satisfied /* probability of  $2^{-54}$  */
4   then
5     for  $2^{13}$  values of  $\blacksquare$  in  $A^{(0)}$  /* 64-2-10-39=13 */
6     do
7       Traversing the  $2^{39}$  values for  $\blacksquare$  in  $A^{(0)}$  while fixing  $\blacksquare$  as a random
          constant, build the table  $U$  with the index of  $c_{\mathcal{R}} \in \mathbb{F}_2^{29}$ .
8       for  $c_{\mathcal{R}} \in \mathbb{F}_2^{29}$  do
9         for  $2^{10}$  values in  $U[c_{\mathcal{R}}]$  do
10          | Compute to the matching point, store them in a list  $L_1$ 
11          end
12          for  $2^{10}$  values of  $\blacksquare$  do
13            | Compute to the matching point  $L_2$ 
14            end
15            for values matched between  $L_1$  and  $L_2$  do
16              | if it leads to the given hash value then
17              |   Output the preimage
18              end
19            end
20          end
21        end
22      end
23 end

```

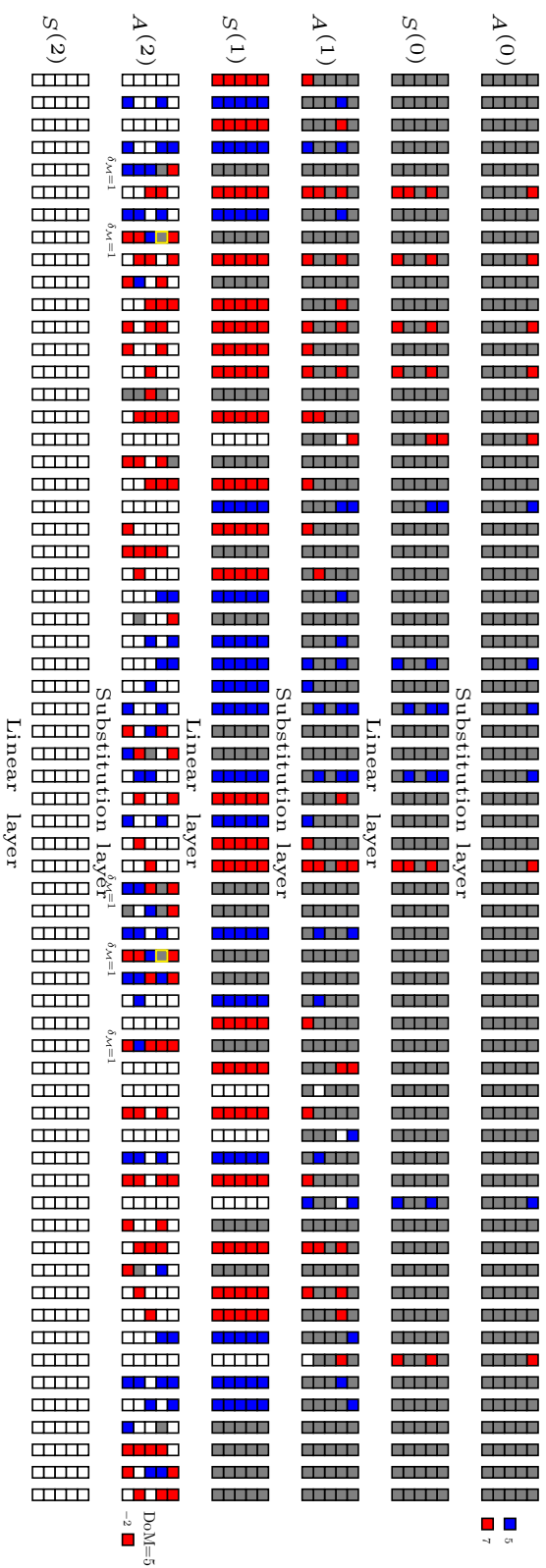


Fig. 26: The experiment on 3-round Ascon-XOF

$$\begin{aligned}
&A_{\{5,1\}}^{(0)} = 1; A_{\{8,1\}}^{(0)} = 1, A_{\{8,3\}}^{(0)} \oplus A_{\{8,4\}}^{(0)} = 1; A_{\{11,1\}}^{(0)} = 1, A_{\{11,3\}}^{(0)} \oplus A_{\{11,4\}}^{(0)} = 1; \\
&A_{\{13,1\}}^{(0)} = 1, A_{\{13,3\}}^{(0)} \oplus A_{\{13,4\}}^{(0)} = 1; A_{\{16,1\}}^{(0)} = 0, A_{\{16,3\}}^{(0)} \oplus A_{\{16,4\}}^{(0)} = 1; \\
&A_{\{19,1\}}^{(0)} = 0, A_{\{19,3\}}^{(0)} \oplus A_{\{19,4\}}^{(0)} = 1; A_{\{26,1\}}^{(0)} = 1, A_{\{16,3\}}^{(0)} \oplus A_{\{26,4\}}^{(0)} = 1; A_{\{28,1\}}^{(0)} = 0; \\
&A_{\{31,1\}}^{(0)} = 0; A_{\{35,1\}}^{(0)} = 1; A_{\{50,1\}}^{(0)} = 1, A_{\{50,3\}}^{(0)} \oplus A_{\{50,4\}}^{(0)} = 1; A_{\{57,1\}}^{(0)} = 1, A_{\{57,3\}}^{(0)} \oplus A_{\{57,4\}}^{(0)} = 1;
\end{aligned}$$

Table 8: Bit Conditions in 3-round Experiment on Ascon-XOF

there are totally 20 conditions on $A^{(0)}$. The degree of matching is counted by the deterministic relations of $A^{(2)}$ according to Observation 3, we get DoM = 5 and list the equations for filtering as Equ. (27).

$$\begin{cases}
A_{\{4,4\}}^{(3)} \cdot A_{\{4,1\}}^{(3)} \oplus A_{\{4,3\}}^{(3)} \oplus A_{\{4,2\}}^{(3)} \cdot A_{\{4,1\}}^{(3)} \oplus A_{\{4,2\}}^{(3)} \oplus A_{\{4,1\}}^{(3)} \cdot A_{\{4,0\}}^{(3)} \oplus A_{\{4,1\}}^{(3)} \oplus A_{\{4,0\}}^{(3)} = S_{\{4,0\}}^{(3)}, \\
A_{\{7,4\}}^{(3)} \cdot A_{\{7,1\}}^{(3)} \oplus A_{\{7,3\}}^{(3)} \oplus A_{\{7,2\}}^{(3)} \cdot A_{\{7,1\}}^{(3)} \oplus A_{\{7,2\}}^{(3)} \oplus A_{\{7,1\}}^{(3)} \cdot A_{\{7,0\}}^{(3)} \oplus A_{\{7,1\}}^{(3)} \oplus A_{\{7,0\}}^{(3)} = S_{\{7,0\}}^{(3)}, \\
A_{\{36,4\}}^{(3)} \cdot A_{\{36,1\}}^{(3)} \oplus A_{\{36,3\}}^{(3)} \oplus A_{\{36,2\}}^{(3)} \cdot A_{\{36,1\}}^{(3)} \oplus A_{\{36,2\}}^{(3)} \oplus A_{\{36,1\}}^{(3)} \cdot A_{\{36,0\}}^{(3)} \oplus A_{\{36,1\}}^{(3)} \oplus A_{\{36,0\}}^{(3)} = S_{\{36,0\}}^{(3)}, \\
A_{\{39,4\}}^{(3)} \cdot A_{\{39,1\}}^{(3)} \oplus A_{\{39,3\}}^{(3)} \oplus A_{\{39,2\}}^{(3)} \cdot A_{\{39,1\}}^{(3)} \oplus A_{\{39,2\}}^{(3)} \oplus A_{\{39,1\}}^{(3)} \cdot A_{\{39,0\}}^{(3)} \oplus A_{\{39,1\}}^{(3)} \oplus A_{\{39,0\}}^{(3)} = S_{\{39,0\}}^{(3)}, \\
A_{\{43,4\}}^{(3)} \cdot A_{\{43,1\}}^{(3)} \oplus A_{\{43,3\}}^{(3)} \oplus A_{\{43,2\}}^{(3)} \cdot A_{\{43,1\}}^{(3)} \oplus A_{\{43,2\}}^{(3)} \oplus A_{\{43,1\}}^{(3)} \cdot A_{\{43,0\}}^{(3)} \oplus A_{\{43,1\}}^{(3)} \oplus A_{\{43,0\}}^{(3)} = S_{\{43,0\}}^{(3)},
\end{cases} \quad (27)$$

Experiments. To make the experiment simple and only test the MITM episode, we carefully set the inner part to make the 20 bit conditions in Table 8 satisfied directly, and only test the MITM episodes. We pre-compute the hash value as the target. We only test one MITM episode, where the other bits exclude \blacksquare and \blacksquare bits in $A^{(0)}$ keep unchanged with the above settings. Similar with Algorithm 2, we need to compute a table of \blacksquare solutions indexed by 2-bit \blacksquare of $A^{(2)}$, $2^5 \times 2^5$ values of \blacksquare and \blacksquare bits are exhausted and filtered with Equ. (27) in the episode. We make the experiment for 32 times with different message blocks and pre-computed targets, and the right values for \blacksquare and \blacksquare bits always remain among the $2^5 \times 2^5 \times 2^{-5} = 2^5$ matched states. The details of the code are also provided at <https://anonymous.4open.science/r/Conditional-MITM-Preimage-Attack>.